Agricultural and Forest Meteorology 297 (2021) 108252

Contents lists available at ScienceDirect

Agricultural and Forest Meteorology

journal homepage: www.elsevier.com/locate/agrformet

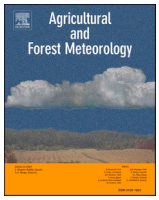

Primary Research

Forest structure and composition drive differences in metabolic energy and entropy dynamics during temperature extremes in longleaf pine savannas

Susanne Wiesner [a,b,c], Gregory Starr [a,*], Lindsay R. Boring [d], Julia A. Cherry [a,e], Paul C. Stoy [b,c,f], Christina L. Staudhammer [a]

[a] Department of Biological Sciences, University of Alabama, Tuscaloosa, AL 35487, USA
[b] Department of Biological Systems Engineering, University of Wisconsin – Madison, Madison, WI 53706 USA
[c] Department of Atmospheric and Oceanic Sciences, University of Wisconsin, Madison, WI 53706, USA
[d] Joseph W. Jones Ecological Research Center, Newton, GA 39870, USA
[e] New College, University of Alabama, Tuscaloosa, AL 35487, USA
[f] Department of Land Resources and Environmental Sciences, Montana State University, Bozeman, MT 59717, USA

ARTICLE INFO

Keywords:
Temperature extremes
Pinus palustris
metabolic energy density
maximum entropy production
freezing
extreme heat

ABSTRACT

The southeastern US has experienced an increase in the number of extreme heat events since the 1970s, due in part to global change. Despite rising temperatures, greater variability in weather has also led to more freeze events across parts of the Southeast, particularly during El Niño winters. Structural variation in forest stands and plant functional diversity can lead to localized micrometeorological differences that may alter the recovery of different forests from these temperature-induced disturbances. This variation can lead to differences in energy and entropy dynamics, which drive the metabolic response of these systems.

Using thermodynamic metrics, we quantified metabolic energy and entropy production in response to extreme heat and freeze events at three longleaf pine savanna sites spanning an edaphic moisture gradient (i.e., xeric, intermediate, mesic). The sites also differed in anthropogenic legacy, with soil tillage occurring at the intermediate site, resulting in greater woody species abundance in the understory and overstory. We found that energy reserves in this ecosystem were built during low precipitation periods and when temperatures were below 20°C. The mesic site, which had the highest plant functional diversity, exhibited an adaptive capacity to temperature extremes by maintaining low metabolic activity throughout temperature disturbances, while the intermediate and xeric sites started with high metabolic activity that gradually declined by ~15% with prolonged temperature extremes. Response to these temperature extremes was a function of hydrological drivers, as lower water availability reduced energy reserves during cold periods and photosynthetic activity during heatwaves – especially at the intermediate and xeric sites as a result of the high energy demand of oaks in the overstory. As climate change continues to alter weather patterns across the globe, it becomes increasingly important to assess metabolic resilience to greater weather variability as a function of ecosystem structure.

1. Introduction

Climate change is intensifying extreme weather events around the globe (Alexander, 2016), placing additional pressures on ecosystems that can drive transitions to alternative states or lead to their collapse (Aitken et al., 2008; Malcolm et al., 2002). The occurrence of extreme heat and freeze events are predicted to further increase across the southeastern United States (Francis et al., 2017; Groisman et al., 2016). Temperature extremes often represent initial disturbances from climate changes (Rahmstorf and Coumou, 2011), making it crucial to assess their effects on ecosystem metabolic processes (Marshall et al., 2003; Pielke et al., 2016). Because ecosystems are constrained by their historic range of meteorological conditions, intensification of extreme weather events can affect their phenological, biophysical and biogeochemical activity (Running & Mills, 2009). However, plant communities within the same ecosystem can respond differently to changes in temperature based on vegetation structure, plant functional types and site legacy (Fig. 1; Paruelo et al., 1999; Binkley et al., 2004; Huxman et al., 2004; Reichstein et al., 2014; Hautier et al., 2015).

The open canopy structures of woodland savannas, for example, can

* Corresponding author: Gregory Starr,
E-mail address: gstarr@ua.edu (G. Starr).

https://doi.org/10.1016/j.agrformet.2020.108252
Received 26 April 2020; Received in revised form 16 November 2020; Accepted 17 November 2020
Available online 29 November 2020

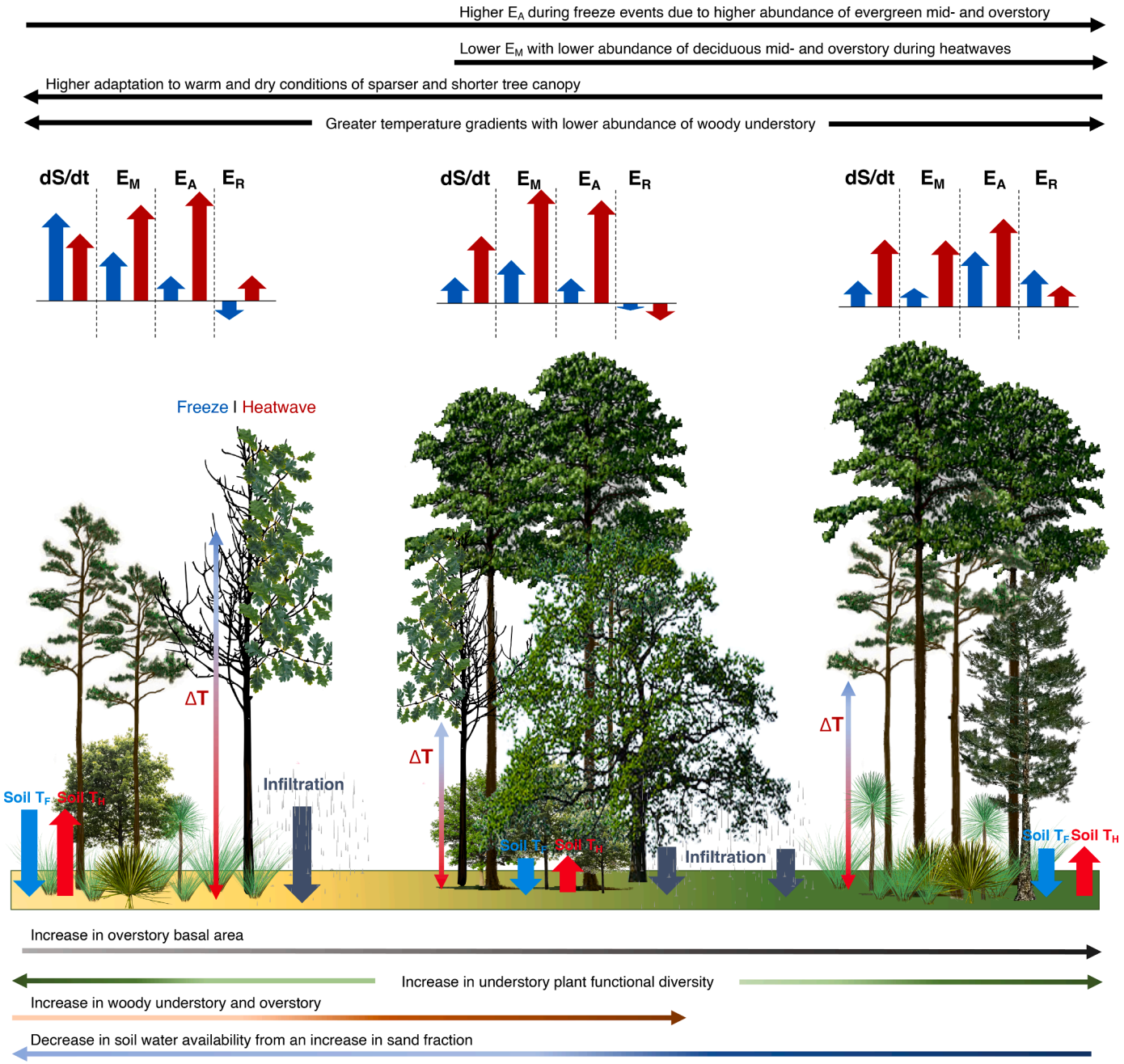

Figure 1. Hypothesized metabolic energy and entropy dynamics during freeze and heatwave events across environmental and structural gradients at three longleaf pine sites, including a xeric, sandy site with low density, short overstory trees (left), an intermediate, woody-dominated site with taller trees (center), and a mesic longleaf pine savanna with higher tree density (right); both the xeric and mesic sites have high native understory plant functional diversity. Top red arrows indicate changes in entropy production (dS/dt), metabolic energy (E_M), available energy (E_A) and energy reserves (E_R) during heatwave events, while top blue arrows indicate changes in dS/dt, E_M, E_A and E_R during freeze events. Lower arrows show changes in soil temperature (soil T_F and soil T_H for freeze and heatwaves, respectively) during temperature extremes and differences in infiltration across sites. Arrows are not drawn to scale. Sites with greater woody understory and overstory maintain higher dS/dt during heatwaves as a result of greater transpiration compared to needle-leaf trees. In contrast, temperature gradients are greater during freeze events at sites with sparser tree canopy and higher oak abundance due to dormant deciduous overstory trees during winter, but lower during summer with greater abundance of woody understory and higher leaf area in the midstory.

create large micrometeorological variation across the ecosystem (Binkley et al., 2004; Hautier et al., 2015; Huxman et al., 2004; Paruelo et al., 1999; Reichstein et al., 2014), which can increase sensitivity to climate drivers such as changes in CO_2, temperature, and precipitation (Fig. 1; Beringer et al., 2011; Rodrigues et al., 2014). As a consequence, different sites may persist through disturbances like heatwaves and droughts (Drake et al., 2018), but may be more affected by prolonged freeze events due to greater environmental gradients based on canopy openness (Fig.1; Boucek et al., 2016). Furthermore, differences in photosynthetic strategies can result in contrasting trends in morphology, physiology and growth in response to climate change. For example, energy and nutrient utilization was enhanced during higher atmospheric CO_2 levels and temperatures in C4 plants (Pugnaire et al., 2019; Peñuelas et al., 2018). To understand how ecosystems respond to extreme weather events, it is important to address how functional diversity and ecosystem metabolic function (i.e., energy acquisition,

utilization and storage; Fig. 1) combine to ameliorate or amplify the effects of temperature disturbances (Alexander, 2016).

Plants have also been shown to alter primary and secondary metabolites production in response to environmental changes, which can disrupt or amplify vegetative and reproductive growth, plant signaling and defenses, which should be evident through alterations of the carbohydrate and energy metabolism of plants (Borghi et al., 2019, Alnsour and Ludwig-Müller 2015). Additionally, altered hydrologic dynamics during extreme heat and freeze events can damage essential photosynthetic machinery, further impacting reproductive success and/or contributing to increased mortality (Frank et al., 2015). Plant water and/or nutrient uptake can cease during extreme heat if transpiration demands to cool vegetative surfaces become too severe or prolonged, or if soil moisture is limited (Ciais et al., 2005; Granier et al., 1999; Reichstein et al., 2003), causing cavitation (Martin-Benito et al., 2017; Savi et al., 2014; Sevanto et al., 2013). These temperature extremes can also cause earlier dormancy in deciduous species, thereby affecting their capacity to acquire energy to persist during winter and/or alter leaf-out the following spring (Fig. 1; Xie et al., 2015). Because interactions among hydrological drivers and temperature extremes can further intensify disturbance effects (Zscheischler et al., 2018), there is a need to understand how "compound effects" alter ecosystem function.

We sought to understand how extreme temperature and hydrologic conditions impact ecosystem energy flux and metabolism. To this end, we quantified ecosystem thermodynamic metrics, including energy reserves (E_R), available energy (E_A) from photosynthetic activity, and metabolic energy density (E_M), which describe how ecosystems utilize available energy through redistribution of nutrients and metabolites, as well as growth processes (Braakman et al., 2017; Chapman et al., 2015). Part of the energy that is dissipated through plant respiration never becomes available to drive other metabolic processes in the plant but can be used in plant leaves for photosynthesis (Silva et al., 2015; Wiesner et al., 2020). Analyzing differences in plant metabolic rates by distinguishing among photosynthesis, dark respiration, or the use of internal energy reserves (Makarieva et al., 2008) permits identification of plants or plant communities that allocate more resources towards energy reserves, thereby improving our understanding of which systems are more resilient to temperature disturbances.

We also quantified entropy metrics, such as entropy production per unit time (dS/dt), to account for differences in ecosystem and biological properties that dissipate energy, which are functions of resource efficiency, plant functional types, and ecosystem structure (Brunsell et al., 2011; Holdaway et al., 2010; Stoy et al., 2014). Variations in structure, like differences in basal area, leaf area or plant species diversity (Fig. 1), can affect the ability of an ecosystem to dissipate energy along these thermodynamic gradients (Kleidon, 2010; Lin, 2015).

In this context, ecosystems that experience frequent disturbances modify E_M in response to lower E_A from climate extremes, such that E_R is conserved (Carturan et al., 2018; Sippela et al., 2016; Villanueva, 2015; Wiesner et al., 2020; Wolf et al., 2016). Ecosystems that accumulate E_R can maintain and restore their structural complexity (i.e., leaf area) following environmental disturbance, which in turn preserves thermodynamic gradients and dS/dt (Figure 1). To the contrary, prolonged imbalances in dS/dt and excessive E_M during disturbances indicate lower adaptive capacity, which may move the system closer to thermodynamic equilibrium (Kleidon, 2012). Because E_M and dS/dt can describe baseline energy efficiencies, they may be especially useful in assessing responses to disturbances in pine savannas and other ecosystems that are particularly susceptible to weather instabilities arising from variation in vegetation structure (Hammond and Winnett, 2009).

To assess ecosystem response to extreme temperatures (i.e., temperatures below the 1st percentile and above the 99th percentile), we quantified metabolic energy density and entropy metrics at three longleaf pine sites spanning an edaphic gradient (mesic, intermediate, xeric). The mesic and xeric sites had the highest understory plant functional diversity but differed in basal area and oak abundance in the overstory because of differences in soil texture and water holding capacity (Fig. 1). Plant functional diversity differed at the intermediate site as a result of historic soil disturbances (i.e., lower abundance of C_4 grasses and greater shrub cover). Because of this variation in ecosystem structure and soil characteristics, we hypothesized that (1) plants at the xeric site use more E_R compared to the mesic and intermediate sites during freeze events as a result of greater temperature fluctuations within its more open canopy, thereby increasing the export of entropy (Fig. 1). Alternatively, (2) plants at the xeric site recover from extreme heat more rapidly than those at other sites because they are better adapted to drier and warmer conditions, as evidenced by a more rapid increase in E_M (Fig. 1, left side), and (3) the intermediate site exhibits a larger decrease in E_R in response to cumulative and/or prolonged temperature extremes because of higher metabolic demand of its shrub understory (Fig. 1, center). Finally, we hypothesized that (4) high rainfall decreases metabolic activity during freeze events at the mesic and intermediate sites because their soil characteristics do not allow for rapid percolation of excess water from the system compared to the xeric site, while lower soil water content intensifies the impact of heat events (Fig. 1, center and right side).

Table 1
Stand characteristics and mean environmental variables (±1 S.D.) for the mesic, intermediate, and xeric longleaf pine study sites at the Joseph W. Jones Ecological Research Center in Georgia, USA. Abbreviations: B_A = Basal Area, DBH = Diameter at Breast Height, LAI = Leaf Area Index, and EVI = Enhanced Vegetation Index.

Stand Characteristics	Mesic	Intermediate	Xeric
B_A all tree spp. (m^2 ha^{-1})	18.4 (±1.7)	17.2(±1.3)	11.1(±2.9)
B_A *P. palustris* (m^2 ha^{-1})	17.4(±2.1)	15.8(±0.9)	8.2(±3.8)
DBH (cm)	25.7 (±15.2)	36.3(±13.7)	18.1(±13.8)
Proportion of oak trees (%)	8.0	7.7	22.0
Wiregrass abundance (%)	28	5	24
Woody plant abundance (%)	12	15	10
Soil drainage	Poorly drained	Well-drained	Excessively well-drained
Water holding capacity (cm per m soil in upper 3 m)	40	28	18
$LAI_{MODIS,\ growing\ season}$ (m^2/m^2)	2.55(±0.7)	2.30(±0.7)	2.27(±0.6)
$LAI_{MODIS,\ non\text{-}growing\ season}$ (m^2/m^2)	1.34 (±0.46)	1.14(±0.39)	1.06(±0.43)
$EVI_{MODIS,\ growing\ season}$	0.418 (±0.046)	0.421 (±0.049)	0.412(±0.049)
$EVI_{MODIS,\ non\text{-}growing\ season}$	0.314 (±0.03)	0.303(±0.03)	0.284(±0.03)

2. Methods

2.1. Site description

This study was conducted from January 2009 through December 2016 at three sites within longleaf pine savanna at the Jones Center at Ichauway (JCI) in southwestern Georgia, USA. All sites are on a two-year prescribed fire interval designed to maintain vegetation structure and ecosystem function. The climate is humid subtropical with a mean annual precipitation of 1310 mm (Kirkman et al., 2001) and temperatures that range from 22°C to 33°C during summer and from 3°C to 16°C during winter (NCDC, 2011).

Longleaf pine ecosystems are considered mesic savannas; globally, savanna ecosystems span rainfall gradients of 800 to 2000 mm y^{-1} (Lehmann et al., 2011; Staver, 2017). Soils across longleaf savannas tend to be nutrient poor and have low N mineralization rates (Wilson et al., 1999), similar to African, Australian, and Asian savannas. Slight differences in soil texture and topography contribute to site-specific edaphic conditions, which lead to differences in ecosystem structure and plant diversity among sites. The mesic site lies on somewhat poorly

drained, sandy loam over sandy clay loam and clay-textured soils with a water holding capacity of 40 cm per m soil (Goebel et al., 2001; 1997). Soils at the intermediate site are well drained and have an argillic horizon of approximately 165 cm with a water holding capacity of 28 cm per m soil (Goebel et al., 1997). The xeric site lies on well-drained, deep sandy soils with no argillic horizon and a water holding capacity of 18 cm per m soil (Addington et al., 2006).

All three sites are situated within 10 km of each other and have elevations ranging from 55 to 65 m. One-hundred-year-old longleaf pine trees (*Pinus palustris* Mill.) dominate the overstory of all sites; however, vegetation structure, based on basal area (B_A, Table 1) and diameter at breast height (DBH), varies by site (Table 1). Oak overstory proportions calculated using basal area estimates (Table 1) range from 7-8 % at the mesic and intermediate sites to 22 % at the xeric site. Based on differences in soil moisture availability, the sites vary in understory composition (Kirkman et al., 2001; 2016). The understory at the mesic and xeric sites is comprised of perennial C_4 grass species including wiregrass (*Aristida beyrichiana* Trin.), as well as forbs, legumes, and ferns and C_3 grasses. Historic soil perturbation (i.e., tillage) at the intermediate site affected species richness, resulting in an understory dominated by woody species (Kirkman et al., 2016; 2001). At the intermediate site, low densities of *Quercus incana* Bartr. and *Q. margaretta* Ashe can be found in the midstory and understory. At the xeric site, scrub oak species *Q. laevis* Walt. and *Q. margaretta* Ashe exist in the overstory, midstory, and understory (Kirkman et al., 2001; Whelan et al., 2013). The sites also differ in mean annual Enhanced Vegetation Index (EVI) and leaf area index (LAI; NASA Land Processes Distributed Active Archive Center and the USGS Earth Resources Observation and Science Center, using MODIS Aqua and Terra data products (MYD13Q1 and MOD13Q1; MCD15A2H and MCD15A3H; DAAC, 2018)). At each of the three study sites, we measured a suite of additional variables from which we could calculate E_A, E_M, E_R, and dS/dt as detailed below.

2.2. Net ecosystem exchange of CO_2 measurements

Net ecosystem exchange of CO_2 (NEE) was measured continuously at all sites using open-path eddy covariance (EC) techniques (Whelan et al., 2013). CO_2 stored directly beneath EC instrumentation was calculated as a function of mean molar CO_2 concentration and measurement height as described in Starr et al. (2016). CO_2 and water vapor concentration were measured with an open-path infrared gas analyzer (IRGA, LI-7500, LI-COR Inc., Lincoln, NE), and three-dimensional (3-D) wind speed and air temperature were measured with a 3-D sonic anemometer (CSAT3, Campbell Scientific, Logan, UT). These sensors were installed ~ 4 m above the canopy at the mesic, intermediate, and xeric sites, corresponding to heights of 34.5, 37.5, and 34.9 m, respectively. The optical path of the IRGA was vertically aligned to match the sampling volume of the sonic anemometer. Both instruments were placed ~ 0.2 m apart to minimize flow distortion between them. Data were logged on CR5000 dataloggers (Campbell Scientific, Logan, UT) and stored on 1 GB CompactFlash cards. The IRGA was calibrated monthly using dry N_2 gas and a gas mixture with known concentration of CO_2, as well as with a dew point generator for H_2O channels (LI-610, LI- COR Inc., Lincoln, NE). Flux data screening was applied to eliminate 30-min fluxes resulting from systematic errors following Starr et al. (2016), such as poor coupling of the canopy with the atmosphere, as defined by the friction velocity (u*), using a threshold < 0.20 m s^{-1}.

Table 2
Descriptions, abbreviations, and calculations for energy density variables.

Definition	Energy component (kJ m^{-2})	Calculations
Photosynthetic energy density from the formation and storage of glucose	E_{in}	(GEE × 0.506 J)/1000
Energy density for ATP and NADPH recycling (35%)	E_{ATP}	(GEE × 0.1771 J)/1000
Maximum available energy density from R_{eco}	E_{max}	(R_{eco} × 0.506 J)/1000
Metabolic energy density	E_M	$E_{max} - E_{ATP}$
Available energy density for metabolic activity	E_A	$E_{in} - E_{ATP}$
Energy reserve (when positive) or use (when negative)	E_R	$E_M - E_A$

2.3. Sensible and latent heat flux measurements

Latent energy (LE) and sensible heat (H) in W m^{-2} were estimated using temperature and 3-D wind speed measurements from the sonic anemometer, as well as water vapor density measurements from the IRGA (Kaimal and Gaynor, 1991). We corrected H and LE fluxes following the Bowen ratio method (Twine et al., 2000), a standard correction method to address potential underestimation of energy fluxes, assuming Bowen ratios (β = H/LE) were correctly measured by the EC systems and using residual energy of net radiation (R_n) when subtracting ground heat flux (Rn − G), as follows:

$$LE = \frac{1}{1+\beta}(R_n - G) \quad (1)$$

$$H = \beta \times LE. \quad (2)$$

2.4. Meteorological instrumentation

The tower recorded various meteorological data, including: incident and outgoing short- and longwave radiation to calculate R_n (NR01, Hukseflux, thermal sensors, Delft, The Netherlands); photosynthetically active radiation (PAR; LI-190, LI-COR Inc., Lincoln, NE); global radiation (LI-200SZ, LI-COR Inc., Lincoln, NE); barometric pressure (PTB110, Vaisala, Helsinki, Finland); air temperature (T_{air}); relative humidity (RH; HMP45C, Campbell Scientific, Logan, UT); precipitation (TE525 Tipping Bucket Rain Gauge, Texas Electronics, Dallas, TX); and wind direction and velocity (Model 05103-5, R.M. Young, Traverse City, MI). All data were stored on CR5000 dataloggers (Campbell Scientific, Logan, UT).

Near the base of each tower, soil volumetric water content (VWC), soil temperature (T_{soil}), and soil heat flux (G) were measured every 15 s. VWC was measured in the top 20 cm of the soil using a water content reflectrometer probe (CS616, Campbell Scientific, Logan, UT). T_{soil} was measured at 4 and 8 cm depths with insulated thermocouples (Type-T, Omega Engineering, INC., Stamford, CT). G was measured at a depth of 10 cm with soil heat flux plates (HFP01, Hukesflux, Delft, The Netherlands). All data were averaged every 30 min on a CR10X datalogger.

2.5. Data processing

Raw EC data were processed using EdiRe (v.1.4.3.1184), which performs a two-dimensional coordinate rotation of the horizontal wind velocities to obtain turbulence statistics perpendicular to the local streamline. Covariance between turbulence and scalar concentrations was maximized through examination of the time series at 0.1 s intervals on both sides of a fixed lag time of 0.3 s. Fluxes were calculated for half-hour intervals and then corrected for the mass transfer resulting from changes in density not accounted for by the IRGA. Barometric pressure data were used to correct fluxes to standard atmospheric pressure. Flux data screening was applied to eliminate 30-min fluxes resulting from any systematic errors following Starr et al. (2016) and Whelan et al. (2013).

Net ecosystem exchange of CO_2 (NEE) was estimated at a time resolution of 30-min, from which gross ecosystem exchange of CO_2 (GEE) and ecosystem respiration (R_{eco}) were calculated as:

$$GEE = -NEE + R_{eco} \quad (3)$$

Missing half-hourly data were gap-filled using separate functions for

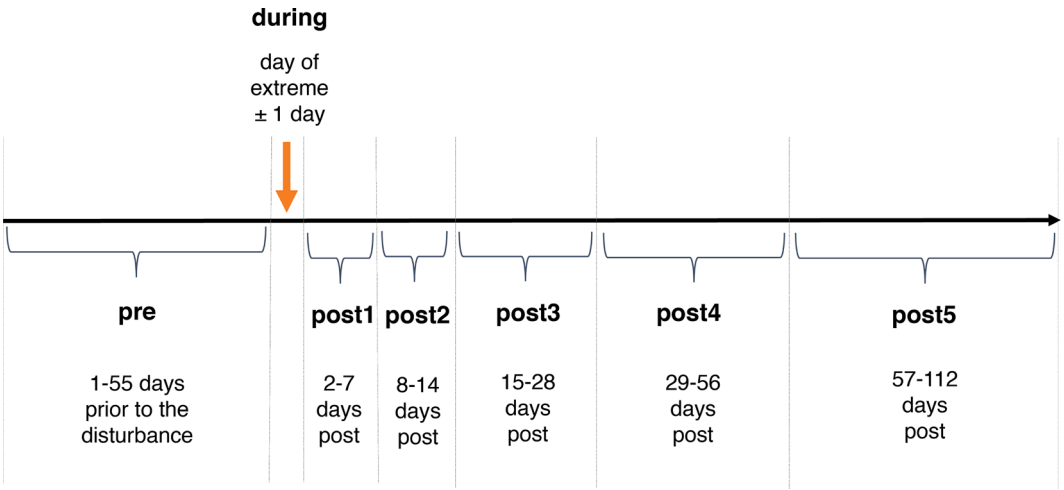

Figure 2. Schematic for cold and heat wave event stage periods (ESPs) used to quantify changes in metabolic activity before, during, and throughout recovery from temperature extremes. Not drawn to scale.

day and night utilizing a Michaelis-Menten approach and a modification of Lloyd and Taylor (1994), respectively, as described in Whelan et al. (2013) and Starr et al. (2016). Annual equations were used to gap-fill data where too few observations were available to produce stable and biologically reasonable parameter estimates; otherwise monthly equations were used.

2.6. Energy density calculations

Energy densities of plant metabolic processes were calculated by relating carbon inputs and outputs to the amount of energy they contain (Table 2). Energy stored in the biochemical reaction of photosynthesis amounts to ~0.506 J μmol^{-1} of CO_2 (Domalski et al., 1986; Nikolov et al., 1995; Schobert, 2013). On average 32-36 adenosine triphosphates (ATPs) are formed during photosynthesis, as recycling of ATP is not always efficient (Silva et al., 2015). Each mole of ATP stores approximately 31.4 kJ, which amounts to 1004 kJ (for 32 ATPs) for each mole of glucose formed. Thus, ~35 % of the ~0.506 J μmol^{-1} produced are solely used for ATP recycling (~0.18 J per μmol CO_2) per mole of glucose (2870 kJ), leaving ~65 % for other metabolic processes (Silva et al., 2015). This conservative estimate includes other energy dissipating processes, such as friction and heat (Schneider and Kay, 1994). By subtracting E_{ATP} from the maximum available energy of energy stored during photosynthesis (i.e., GEE = E_{in}), we obtain ~0.35 J per μmol CO_2 for metabolic energy density, which is used for plant functions and growth (E_M, ~65 % of E_{in}). For the analysis, we used ratio E_M, E_A and E_R (E_A-E_M), to quantify changes in energy dynamics during temperature extremes.

2.7. Entropy production calculations

We quantified entropy production and fluxes of the shortwave (R_s) and longwave (R_l) radiation following Brunsell et al. (2011), Holdaway et al. (2010), and Stoy et al. (2014). The sum of the total daily entropy flux (J) in kJ m^{-2} K^{-1} day^{-1} was calculated by adding all entropy fluxes between the surface and the atmosphere as:

$$J = J_{Rl} + J_{Rs} + J_{LE} + J_H + J_G + J_{GEE} + J_{Reco} + J_{LEmix} \quad (4)$$

Detailed descriptions of the calculations for each of the entropy fluxes used to calculate J are provided in the Appendix.

The conversion of low entropy R_s and R_l to high entropy heat (σ_{Rs} and σ_{Rl}, respectively) in kJ m^{-2} K^{-1} at the surface through the absorption of shortwave radiation was calculated using surface temperature (T_{srf} in K, Eq. A3) and sky temperature (T_{sky} in K, Eq. A4) and the temperature of the sun (T_{sun}; ~5780 K) as:

$$\sigma_{Rs} = R_{s,net} \times \left(1 / T_{srf} - 1 / T_{sun}\right) \quad (5)$$

and

$$\sigma_{Rl} = R_{l,in} \times \left(1 / T_{srf} - 1 / T_{sky}\right). \quad (6)$$

The overall daily entropy production (σ) in kJ m^{-2} K^{-1} was calculated as the sum of the entropy productions of shortwave and longwave radiation:

$$\sigma = \sigma_{Rl} + \sigma_{Rs} \quad (7)$$

where σ was partitioned using EVI as an approximation for fractional vegetation cover to account for the difference in absorbed radiation on leaf and non-vegetated surfaces (Wiesner et al., 2019). Entropy production of non-vegetated surfaces (σ_{land}) was estimated as:

$$\sigma_{land} = (1 - \mathrm{EVI}) \times \sigma. \quad (8)$$

We calculated entropy production on leaf surfaces (σ_{leaf}, Eq. 9) as the sum of entropy production (σ_{PAR} Eq. A7) from absorbed photosynthetic active radiation (FPAR in W m^{-2}, Eq. A8) and entropy production from the remainder of R_s—PAR ($\sigma_{Rs,leaf}$, Eq. A9), assuming all absorbed energy was converted into heat. Finally, we included $\sigma_{Rl,leaf}$ to account for entropy production from longwave radiation absorbed on leaf surfaces (Eq. A10).

$$\sigma_{leaf} = \sigma_{PAR} + \sigma_{Rs,leaf} + \sigma_{Rl,leaf} \quad (9)$$

The daily change in entropy (dS/dt) in kJ m^{-2} K^{-1} was calculated from the entropy flux and radiative entropy production:

$$\mathrm{dS}/\mathrm{dt} = \mathrm{J} + \sigma_{land} + \sigma_{leaf} \quad (10)$$

Negative dS/dt values indicate an export of entropy from the ecosystem to its surroundings. With these calculations, we are not considering any entropy transport or production associated with rainfall, which was similar among study sites, or soil water transport (Kleidon and Schymanski, 2008, Brunsell et al. 2011).

2.8. Statistical analyses

We identified freeze and heat wave events using the extreme ends of the observed air temperature (T_{air}) frequency distribution. For freeze events, we used dates containing half hours of T_{air} below 0 °C; which represented temperatures below the 1st percentile. For extreme heat

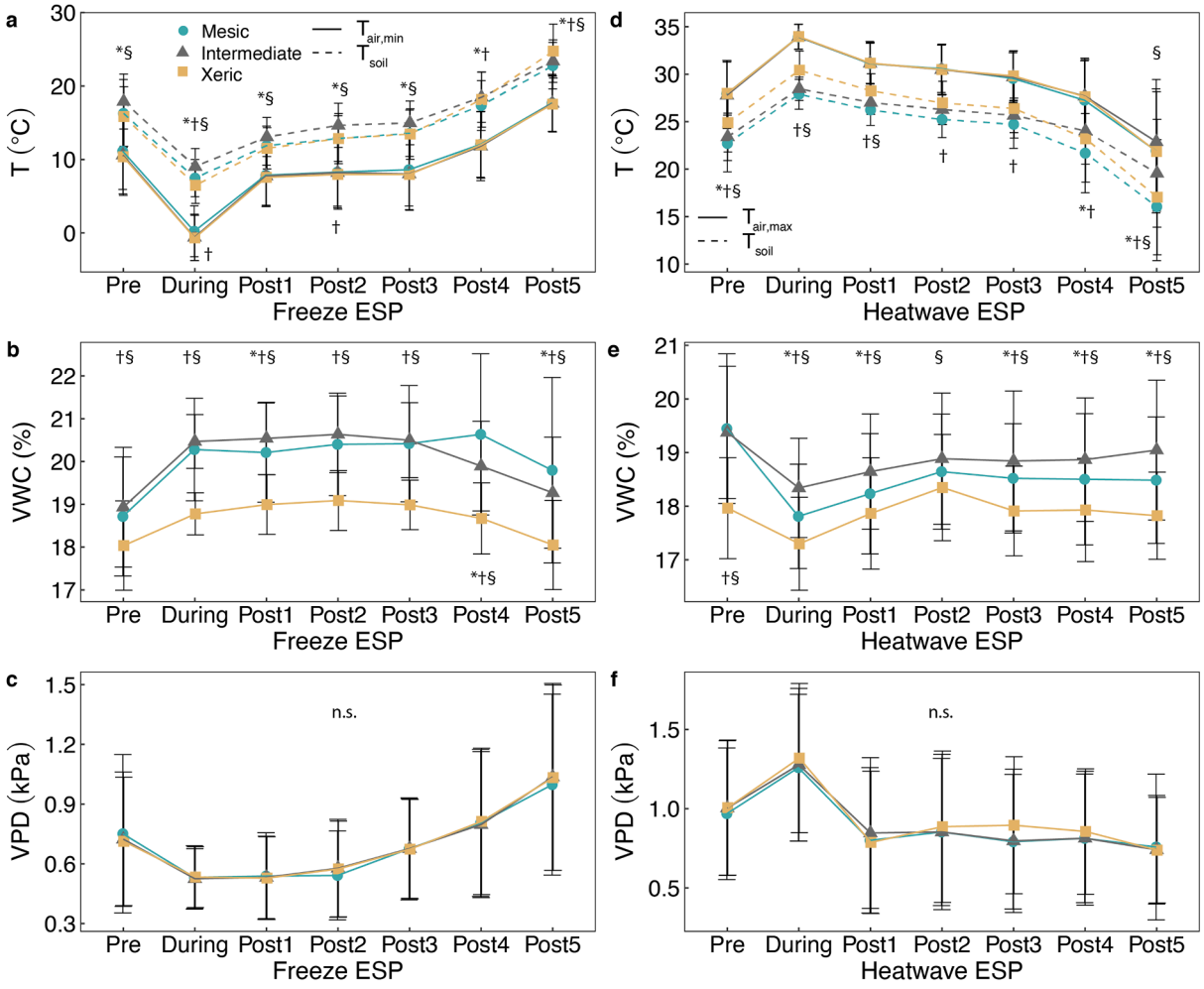

Figure 3. Average (± 1 S. D.) daily values of environmental variables: (a) minimum air temperature (T_{min} in °C) and soil temperature (T_{soil} in °C); (d) maximum air temperature (T_{max} in °C) and soil temperature (T_{soil} in °C); (b, e) soil volumetric water content (VWC in %); and (c, f) vapor pressure deficit (VPD in kPa) at the mesic, intermediate, and xeric sites during freeze (a-c) and heat (d-f) event stage periods (ESPs), which are defined as: pre (56 days prior to the extreme event), during (1 day prior to and post- disturbance), and post1-5 (7, 14, 28, 56 and 112 days post event, respectively). Symbols show significant differences of average energy densities and entropy changes between (*) the mesic and intermediate sites, (§) the mesic and xeric sites, and (†) the intermediate and xeric sites. For panels a and d, symbols for respective temperatures are above and below each respective measurement (i.e., T_{soil}, T_{min} and T_{max}).

events, we used dates where half hourly T_{air} was above the 99th percentile of 30 °C.

For each extreme event, we identified seven "event stage periods" (ESP) to analyze the range of ecosystem recovery times at the three sites and associated environmental covariates. The ESP "during" encompassed the date of the respective temperature extreme plus one day prior to and one day following the event to incorporate possible overlap (Figure 2). The ESP "post1" encompassed the next 7 days after the event, beyond the "during" period. ESPs "post2", "post3", "post4" and "post5" encompassed the next 14, 28, 56 and 112 (non-overlapping) days, respectively (Figure 2). We found no significant change when we considered periods beyond 112 days past the events; hence, 112 days (post5) was determined to be the maximum time of recovery from freeze and extreme heat at the three sites.

We also included a pre-event period ("pre") encompassing 56 days prior to each temperature extreme. The pre-event contained only days that did not overlap with the other ESP categories. We tested the sensitivity of models to the definition of pre-event period length but found no significant differences in results. We also included a binary indicator for cumulative effects ("cumulative effect") of heat and freeze events when they occurred while the sites were recovering (i.e., during "post" ESPs) to account for a possible overlap of temperature extreme ESPs. This allowed us to assess the metabolic response at the three sites when temperature extremes occurred more frequently. To assess the impacts of prolonged temperature extremes, we included a continuous variable describing the length, a measure of intensity (INT), of extreme events encompassing ESPs "during", "post1" and "post2".

Prior to testing our study hypotheses, we formulated simple linear mixed models to describe how T_{air}, minimum daily air temperature (T_{min}), maximum daily air temperature (T_{max}), T_{soil}, VWC, vapor pressure deficit (VPD), and rainfall related to site, the respective temperature extreme categories, INT, and their interactions with site. We included a random effect for the interaction of year and month to account for variation among years.

We then formulated models for four dependent variables to describe freeze and heat extremes (eight models total). These models quantified changes in E_A, E_M, E_R, and dS/dt. Models included T_{min} and T_{max} for cold and heatwaves, respectively, VWC, VPD, and daily rainfall sums (rain) as independent variables. In addition, we included factors for site, freeze and heat ESPs, cumulative effects, and a continuous variable for event length. We also included interactions of site with the cumulative effect indicator, INT, and interactions of site and ESP with T_{min} or T_{max}, VWC, VPD, and rainfall, as well as three-way interactions of freeze or heat ESP, with site and T_{min} or T_{max}, or VWC to account for the influence of other

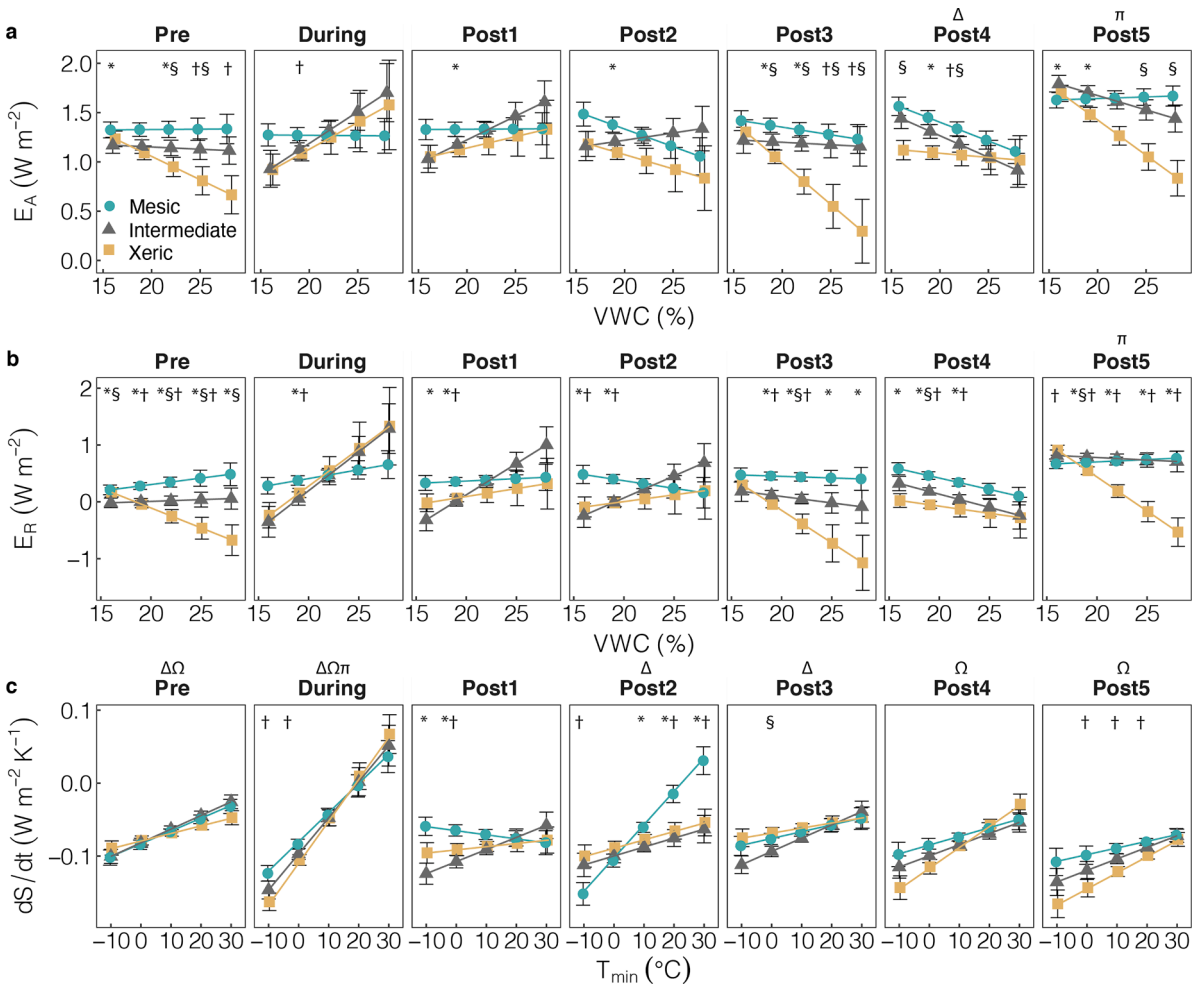

Figure 4. Least square mean predicted values from mixed model (Table A3) for three-way interactions of site and event stage period (ESP) with (a) volumetric water content (%) on available energy (E_A, W m^{-2}), (b) volumetric water content (%) on energy reserves (E_R, W m^{-2}) and (c) minimum air temperature (T_{min}) on entropy production (dS/dt) for freeze events. ESPs are defined such that "pre" encompasses the 56 days prior to the disturbance, "during" encompasses the period from 1 day prior to 1 day post-disturbance, and "post1-5" encompass 7, 14, 28, 56 and 112 days following weather extremes, respectively. Symbols indicate significant differences of average (± 1 S. D.) energy densities and entropy changes between (*) the mesic and intermediate sites, (§) the mesic and xeric sites, and (†) the intermediate and xeric sites, as well as significant changes (decrease or increase) of energy densities and entropy changes by environmental variables (Δ) for the mesic site, (Ω) the intermediate site, and (π) the xeric site.

environmental drivers by site during extreme temperature events. We quantified significant differences for the interactive effects using post-hoc tests with Tukey adjustments using the *lsmeans* package in R and RStudio (Lenth, 2016; R Core Team, 2013).

3. Results

3.1. Duration of extreme events

During the 7 years of this study, the mesic, intermediate and xeric sites experienced extreme freeze events for a total of 197, 161 and 164 days, respectively, most of which occurred during January and February. Of these freeze events only 8 days were isolated events at each site; 30 days of freeze events overlapped with ESP post5 at the mesic site, whereas only 15 days were overlapping with ESP post5 at the intermediate and xeric sites. Extreme freeze events ($T_{air} < 0$ °C) lasted on average for 14 hours, and up to 24 hours per day. Their durations ranged from 3-14 days during winter months of each year of the study, with longer events occurring in 2009, 2010 and 2013. Extreme heat events ($T_{air} > 30$ °C) occurred for a total of 205, 230 and 212 days, respectively, mainly from June through August. For heatwaves, most events overlapped, except for 4 isolated days at each site. For 23-27 days of the total days, depending on the site, heatwaves overlapped with the recovery ESP post5. On average, extreme heat events lasted 7 hours during each day that they occurred, with a maximum length of 20 hours. The average duration of each of these extreme events was 6 days; however, we did observe two longer heat events that lasted 12 and 17 consecutive days in June through August of 2010 and 2011, respectively.

3.2. Environmental differences among sites

Air temperature (T_{air}) and T_{min} were not significantly different among sites for freeze event ESPs, but significantly decreased with increased freeze intensity at the intermediate and xeric sites (by ~5 °C; Figure 3a). Soil temperature (T_{soil}) was significantly lower (~3°C) at the mesic and xeric sites compared to the intermediate site for cold wave ESPs pre through post3 (Figure 3a). For freeze events, the xeric site had significantly lower VWC (Figure 3b). Vapor pressure deficit (VPD) was not significantly different among sites for cold wave ESPs (Figure 3c).

During heatwave ESPs, T_{air} and T_{max} were not significantly different among sites and did not change with increasing heat intensity (Figure 3d). During extreme heat, T_{max} reached up to 35°C at all sites. T_{soil} at the mesic site was significantly lower (by ~ 1-3°C) compared to the xeric site for heat ESPs pre through post1. The intermediate site had

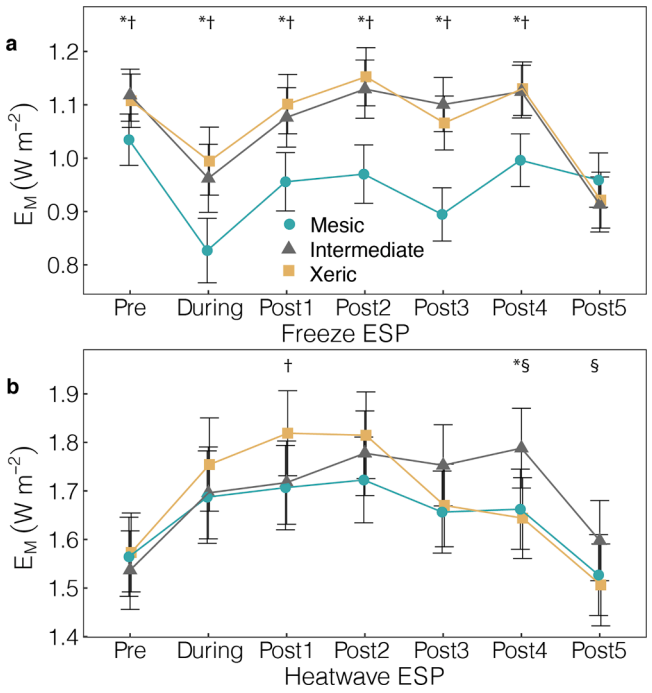

Figure 5. Least square mean predicted values from mixed model for the two-way interactions of site and event stage period (ESP) on metabolic energy (E_M, W m^{-2}) during (a) freeze (Table A3) and (b) heat wave (Table A4) events. ESPs are defined such that "pre" encompasses the 56 days prior to the disturbance, "during" encompasses the period 1 day prior to 1 day post-disturbance, and "post1-5" encompass 7, 14, 28, 56 and 112 days following the weather extremes, respectively. Symbols show significant differences of average (±1 S.D.) energy densities and entropy changes between (*) the mesic and intermediate sites, (§) the mesic and xeric sites, and (†) the intermediate and xeric sites, as well as to describe significant changes (decrease or increase) of energy densities and entropy changes by environmental variables (Δ) for the mesic site, (Ω) the intermediate site, and (π) the xeric site.

significantly higher T_{soil} compared to the mesic site prior to the heatwaves (1°C; Figure 3d).

For the heat ESPs pre and during, the xeric site had significantly higher T_{soil} compared to the intermediate site. VWC significantly decreased at the mesic and intermediate sites during extreme heat events, but not at the xeric site. VWC increased by ~1% until post2 at all sites following extreme heatwaves. VWC was significantly higher at the intermediate site (up to 1.5%) than the mesic and xeric sites for heat ESPs during, post1-3, and post5 (Figure 3e). For heat ESPs pre and post3-5, the mesic site had significantly higher VWC compared to the xeric site. Rainfall and VPD did not differ among sites during freeze or heat ESPs (Figure 3c,f; Tables A2 and A3).

EVI was significantly lower at the xeric site compared to the other sites for freeze ESPs pre through post1 (by ~0.02-0.04; Figure A1(a)), while EVI during heatwaves was only significantly lower at the xeric site compared to the other sites for ESP post5 (Figure A1(a)). Leaf area indices were significantly higher at the mesic site for freeze ESPs pre through post4. LAI for heatwave ESPs was only significantly larger at the mesic site compared to the xeric site for ESPs during through post3 (~ by 0.3 m^2 m^{-2}; Figure A1(b) and (d)), whereas the intermediate site had significantly lower LAI compared to the other sites prior to heatwave events.

3.3. Lagged effects of cold wave events on metabolic processes

Available energy (E_A) was significantly higher (~1-1.5 W m^{-2}) during post5 compared to all other cold wave ESPs when VWC was below 22% at the mesic, intermediate, and xeric sites (Figure 4a). E_A decreased significantly with an increase in VWC at the mesic site during post4 (by ~0.5 W m^{-2}) and during post5 at the xeric site (below 0.5 W m^{-2}). For low VWC (19%), the mesic site had significantly higher E_A (~0.4 W m^{-2}) compared to the xeric site during cold wave events. When VWC was between 19 and 22% the mesic site had significantly higher E_A compared to the intermediate and xeric sites for cold ESPs post3-5 and prior to cold waves. When VWC increased above 22%, E_A was significantly lower at the xeric site compared to the other two sites prior to cold waves and during post5.

Models of metabolic energy indicated no significant interactive effect of temperature or VWC with site or freeze ESPs (Table A3). E_M was lower at the mesic site compared to the intermediate and xeric site from cold wave ESPs pre through post4 (by 0.1-0.2 W m^{-2}; Figure 5a). E_M significantly decreased only at the mesic site during freeze events (to 0.8 W m^{-2}), followed by a significant increase 7 days post freeze. E_M was significantly higher at the intermediate and xeric sites two weeks following the freeze compared to during the cold wave.

Prior to freeze events, contrary to our hypothesis 1, energy reserves (E_R) were significantly higher at the mesic site (by ~0.3-1 W m^{-2}) compared to the other two sites when VWC was greater than 19%. E_R were significantly different at all sites from pre through post4 compared to post5 when VWC was below 22%. E_R were significantly higher at the mesic site during cold wave events and during the following 7 and 14 days (by 0.5 W m^{-2}), compared to the intermediate and xeric sites when VWC was below 19%. Both the intermediate and xeric sites had negative E_R when VWC was below 19% during cold waves (Figure 4b). E_R decreased at the xeric site when VWC increased following cold events (post5).

Daily change in entropy (dS/dt) was significantly less negative at all sites during freeze events when minimum air temperatures increased (ranging from –0.15-0.05 W m^{-2} K^{-1}), as well as prior to freeze events at the mesic and intermediate sites (Figure 4c). dS/dt became less negative during post2, post3, and post4 at the mesic, intermediate, and xeric sites, respectively, when minimum temperature increased.

3.4. Lagged effects of extreme heat on metabolic processes

E_A significantly increased with greater VWC at the mesic site during post2-4 and at the intermediate site during heatwave events, while E_A at the xeric site significantly decreased prior to heat events with greater VWC (> 19%), resulting in lower E_A compared to the other two sites (Figure 6a; Table A4). E_A was significantly lower at the mesic site compared to the intermediate site during heatwave events when VWC was above 19% and compared to the other two sites 14 days post heatwaves for lower VWC. When VWC increased above 19% during post3, 4, and 5, E_A at the mesic site was significantly higher compared to the intermediate site. There were no significant differences in E_A among heatwave periods at the mesic and xeric sites when VWC was above 19%, except during heatwaves when E_A was greater at the xeric site compared to pre (VWC > 22%). For VWC below 19%, E_A was significantly higher at the mesic, intermediate, and xeric sites prior to heatwaves compared to all other heatwave ESPs. For VWC of 19%, E_A at the intermediate site was significantly higher during post1 and 2 compared to post3-5.

The three-way interactions of site, heatwave ESP, and T_{max} or VWC were not significant in the E_M model, but the two-way interaction of site and heatwave ESP indicated that E_M at the intermediate site was significantly higher during post4 compared to the other two sites (Figure 5b). The mesic site had significantly lower E_M compared to the xeric site 7 days post the heatwave events, in support of hypothesis 2. E_R decreased at the mesic and intermediate sites prior to heatwave events, and at all sites during post5 with an increase in T_{max} (Figure 6b). E_R at the xeric site were significantly lower compared to the other two sites when T_{max} was below 30 °C and significantly higher at the mesic site compared to the other two sites during post5 when T_{max} was below 40°C. During post3 and 4, E_R at the intermediate site were significantly

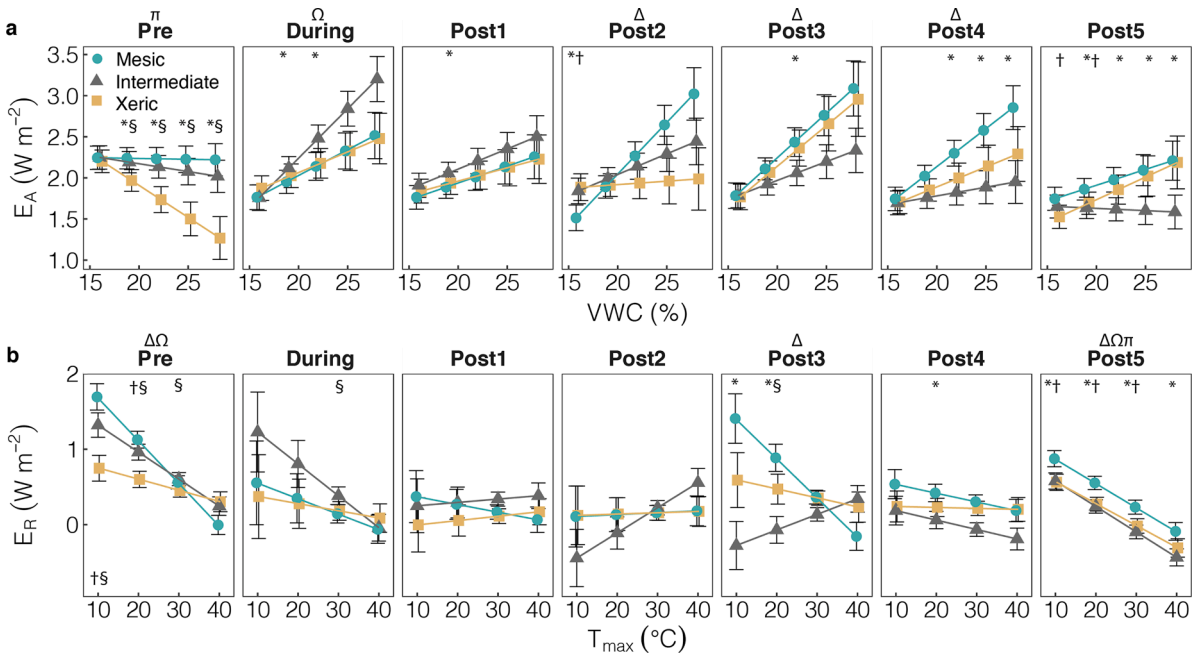

Figure 6. Least square mean predicted values from mixed model for the three way interactions of site and event stage period (ESP) with (a) volumetric water content (VWC, %) on available energy (E_A, W m^{-2}) and (b) maximum air temperature (T_{max}) on energy reserves (E_R, W m^{-2}) for heatwave events (Table A4). ESPs are defined such that "pre" encompasses the 56 days prior to the disturbance, "during" encompasses the period 1 day prior to 1 day post-disturbance, and "post1-5" encompass 7, 14, 28, 56 and 112 days following the weather extremes, respectively. Symbols show significant differences of average (± 1 S. D.) energy densities and entropy changes between (*) the mesic and intermediate sites, (§) the mesic and xeric sites, and (†) the intermediate and xeric sites, as well as to describe significant changes (decrease or increase) of energy densities and entropy changes by environmental variables (Δ) for the mesic site, (Ω) the intermediate site, and (π) the xeric site.

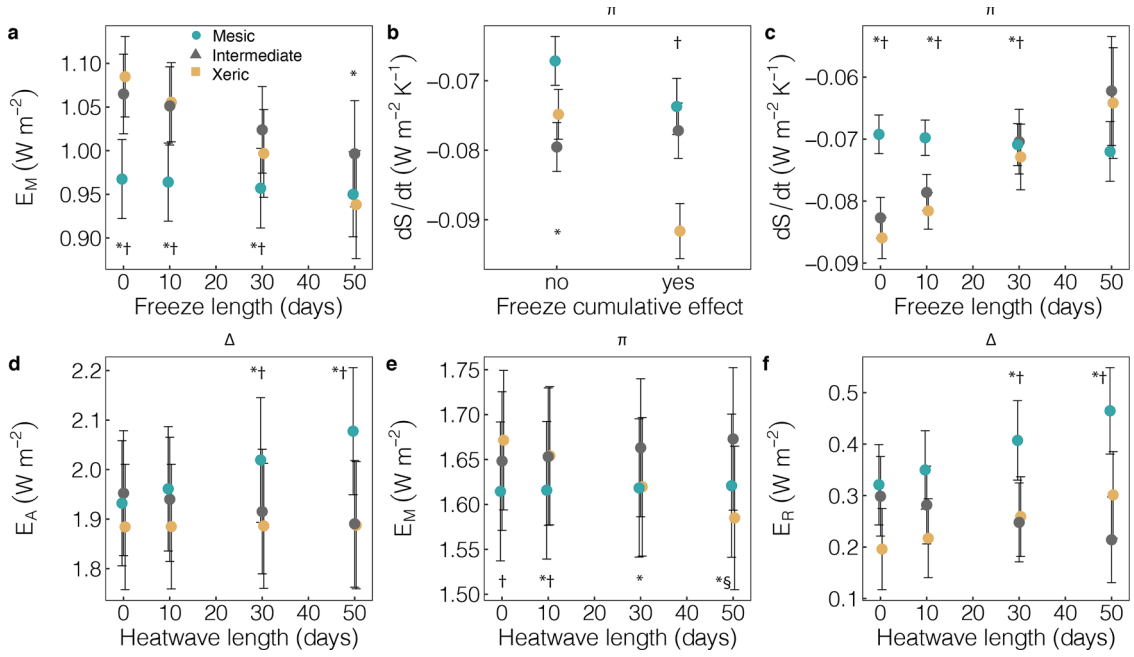

Figure 7. Least square mean predicted values from mixed model results as a function of cumulative effect (cumulative effect) and event length (cold wave/heatwave length, INT) for (a-c) freeze (Table A3) and (d-f) heat events (Table A4) for the interactions of (a) metabolic energy (E_M) and INT, (b) entropy change (dS/dt) with cumulative effect, and (c) dS/dt with INT, as well as for the interactions of (d) available energy (E_A), (e) metabolic energy (E_M), and (f) energy reserves (E_R) with INT. The interaction of INT and site for heat events on E_M was not significant in the model. Symbols show significant differences of average (± 1 S. D.) energy densities and entropy changes between (*) the mesic and intermediate sites, (§) the mesic and xeric sites, and (†) the intermediate and xeric sites, as well as to describe significant changes (decrease or increase) of energy densities and entropy changes by environmental variables (Δ) for the mesic site, (Ω) the intermediate site, and (π) the xeric site.

lower compared to the other two sites when T_{max} was between 10 and 30°C. For T_{max} below 20°C, the mesic and intermediate sites had significantly higher E_R prior to heatwaves compared to post1, 2, 4 and 5, and post1-5, respectively. For greater T_{max}, E_R were significantly lower at the mesic site during heatwaves compared to periods leading up to heat events, whereas the intermediate site had lower E_R during post5 compared to all other ESPs, when T_{max} was between 30-40°C. The xeric site had lower E_R during post5 compared to pre and post1-4 when T_{max} was above 30°C, but showed no significant differences in E_R for other periods or temperatures, in further support of our hypothesis 2. The two-way interaction of heatwave ESP and site, as well as three-way interactions of ESP, site, and environmental variables, were not significant in the model of dS/dt.

3.5. Cumulative effects of cold and heat wave events on metabolic processes

Cumulative and event length effects were not significant in the models of E_A and E_R. An increase in cold event length significantly decreased E_M only at the xeric site (by 0.1 W m^{-2}; Figure 7a). E_M was significantly lower at the mesic site compared to the other sites when freeze event length was shorter than 30 days. dS/dt became significantly more negative at the xeric site (< –0.09 W m^{-2} K^{-1}) when cold wave events became cumulative (Figure 7b), and was significantly more negative compared to the other sites. The intermediate and xeric sites had significantly more negative dS/dt compared to the mesic site when freeze event length was shorter 30 days (Figure 7c).

Cumulative effects only decreased E_M during heatwave events, and were not significantly different by site (Table A4). An increase in heatwave length significantly increased E_A only at the mesic site (to 2.1 W m^{-2}; Figure 7d), which resulted in significantly higher E_A compared to the other sites when heatwave length was over 30 days. For heatwaves up to 30 days, the mesic site had significantly lower E_M compared to the xeric site and compared to the intermediate site when heatwaves were longer than 10 days (Figure 7e). With an increase in heatwave length, E_R significantly increased only at the mesic site (by ~0.15 W m^{-2}; Figure 7f), which resulted in significantly higher E_R compared to the intermediate and xeric sites when heatwave length was over 30 days, in support of hypothesis 3.

3.6. Environmental drivers of metabolic processes during freezes

In support of hypothesis 4, E_A significantly decreased with an increase in rainfall (Figure A2(a)), especially at the intermediate site (below 0.75 W m^{-2}), whereas the mesic site had significantly higher E_A compared to the other two sites when rainfall as below 200 mm per day (~0.9 W m^{-2}). E_M significantly increased only at the xeric sites with an increase in VWC (Figure A2(b)), resulting in greater E_M compared to the other two sites when VWC was above 20% (by ~0.3 W m^{-2}). Rain increased E_M at all sites (by ~0.4-0.6 W m^{-2}), but more so at the intermediate site. E_R significantly decreased at all sites as rain increased (Figure A2(c)), further supporting hypothesis 4. E_R were significantly more negative at the intermediate site when rain increased above 50 mm per day (–1 W m^{-2}) and were significantly higher at the mesic site when rainfall was below 50 mm (0.5 W m^{-2}; Figure A2(d)). T_{air}, rainfall, and VWC did not significantly affect the magnitude of dS/dt at the sites, but dS/dt significantly decreased, becoming more negative (below –0.2 W m^{-2}) as VPD increased, but more so at the intermediate and xeric sites (Figure A2(e)).

E_A significantly increased for all freeze ESPs when T_{min} and VPD increased (by ~0.25 W m^{-2} and 2 W m^{-2}, respectively; Figure A3(a) and (c)), but the opposite was found when rainfall increased, especially during cold wave events (decrease below ~0.5 W m^{-2}; Figure A3(b)). E_M significantly increased with greater daily rainfall (by ~0.5 W m^{-2}; Figure A3(d)) for all cold wave ESPs, but VPD only significantly increased E_M for post4 and 5 (Figure A3(e)). An increase in T_{min} resulted in lower E_R (Figure A3(f)), with positive E_R when T_{min} was below 20°C (ranging from –1 to 1.5 W m^{-2}). Rainfall decreased E_R to negative (below –0.5 W m^{-2}; Figure A3(g)) for all freeze ESPs, but E_R during post5 remained positive up to 100 mm of rainfall per day. VPD significantly increased E_R for all cold wave ESPs (by ~2 W m^{-2}; Figure A3(h)). dS/dt significantly decreased becoming more negative for all cold wave ESPs when VPD increased (below –0.1 W m^{-2}; Figure A3(i)).

3.7. Environmental drivers on metabolic processes during extreme heat

Changes in E_A during heatwave ESPs were not significantly different among sites with changes in T_{max}, rainfall, or VPD. E_M significantly increased at all sites with increases in T_{max} (2 W m^{-2} when T_{max} reached 40°C; Figure A4(a)), with lower E_M at the mesic site when T_{max} was below 20°C. E_M significantly increased with higher VWC only at the xeric site, in partial support of hypothesis 4, resulting in greater E_M (by up to 0.4 W m^{-2}) at the xeric site when VWC was above 22% (Figure A4(b)). E_R significantly increased only at the mesic site when VWC increased (Figure A4(c)), further supporting hypothesis 4. E_R were lowest at the xeric site (~ 0 W m^{-2}) when VWC was > 25% and highest at the mesic, which was also significantly higher (0.6 W m^{-2}) than the intermediate site (0.3 W m^{-2}). dS/dt significantly decreased, becoming more negative when VPD increased, with a greater increase at the intermediate and xeric sites (-0.25 W m^{-2} K^{-1}), such that the mesic site had lower entropy exports (-0.19 W m^{-2} K^{-1}; Figure A4(d)). dS/dt significantly decreased at the intermediate site with an increase in rainfall, resulting in lower entropy exports (-0.07 W m^{-2} K^{-1}) compared to the mesic (-0.09 W m^{-2} K^{-1}) and xeric (-0.08 W m^{-2} K^{-1}) sites (Figure A4(e)).

E_M significantly increased with greater T_{max} for all heatwave ESPs (Figure A5(b)), whereas rainfall increased E_M only for ESPs pre, post1 and post5, resulting in significantly greater E_M (by 0.25 W m^{-2}) during post1 compared to post4, when rainfall was greater than 100 mm per day. Higher rainfall resulted in lower E_A during all heatwave ESPs (Figure A5(a)). E_A increased with greater T_{max} and VPD for all heatwave ESPs, where post5 had the lowest values of E_A compared to other ESPs (Figure A5(c)). An increase in T_{max} increased E_M (Figure A5(d)). Higher rainfall only significantly increased E_M for heatwave ESPs pre, post1, and post5 (Figure A5(e)). VPD significantly decreased E_M only for heatwave ESPs pre, during, post4, and post5, resulting in lower E_M (by 0.5 W m^{-2}) compared to all other ESPs when VPD was > 1 kPa (Figure A5(f)). Higher VWC significantly decreased E_R prior to heatwave events, whereas greater VWC significantly increased E_R during heatwave events (Figure A5(g)). An increase in rainfall significantly decrease E_R to negative for all heatwave ESPs, except during heatwave events, such that high rainfall resulted in greater E_R (> 0 W m^{-2}) compared to post5 when rainfall was above 100 mm per day (Figure A5(h)). Similarly, higher VPD significantly increased E_R for all heatwave ESPs (Figure A5(i)), except during heat events, which had lower E_R compared to post5 (from 0.5-1 W m^{-2}). Heatwave ESP pre had significantly higher E_R compared to post1-4 when VPD increased above 1 kPa. dS/dt became significantly more negative with an increase in rainfall only for heatwave ESP post4, whereas higher VPD resulted in more negative dS/dt for all heatwave ESPs, with a greater slope during heatwave events (Figure A5(j-l)).

4. Discussion

Extreme weather events are becoming more frequent globally with climate change (Alexander, 2016). The southeastern US is particularly threatened by these changes, as both heat and freeze events are expected to increase in intensity (Francis et al., 2017; Groisman et al., 2016). Here, we used thermodynamic metrics to understand how longleaf pine ecosystems that differed in hydrology, basal area, and understory plant functional diversity respond metabolically to temperature extremes. We showed that metabolic energy efficiency and entropy production

differed among three pine savanna sites that differ in soil moisture, vegetation structure, and plant functional diversity. Even though entropy metrics were a useful tool to identify differences in resource efficiency among sites, the metrics of metabolic energy more clearly described the sites' strategies to recover from extreme temperatures by elucidating how sites acquired, stored, and expended energy.

4.1. Metabolic energy adaptation during cold wave events and throughout recovery

In support of our first hypothesis, metabolic activity at the xeric site was more affected by freeze events, as dS/dt increased and E_M decreased when events accumulated. Greater metabolic variation during freeze events was likely the result of lower basal area, which resulted in greater temperature fluctuations during colder months when deciduous oak trees were dormant (Latimer and Zuckerberg, 2017). In addition, lower VWC at the xeric site contributed to lower soil heat capacity at the site (Abu-Hamdeh, 2003), which decreased soil temperatures more drastically during freeze events and may have intensified the effect of cold stress. As a result, the xeric site relied on E_R following freezes, as its higher proportions of deciduous oak trees utilized more reserves during winter and spring leaf development (Bazot et al., 2013). A similar effect was seen at the intermediate site; however, E_R were lower compared to the xeric site following freeze events when soil water availability was low. Nevertheless, higher photosynthetic capacity of oak trees during warmer months (Richardson et al., 2010; 2013) was consistent with greater E_R when VWC was optimal (< 20%), which compensated for the resource demands of winter (Bazot et al., 2013). At the mesic site, E_M declined by 20% during freeze events, suggesting mesic sites respond with energy conservation and restricted growth during low temperatures, consistent with the overwintering strategies of more cold-hardy coniferous trees (Lenz et al., 2016).

4.2. Metabolic energy adaptation during heatwave events throughout the recovery

Rainfall and soil moisture availability were important drivers of metabolic processes in the pine savannas during extreme heat events. The intermediate site was less efficient in cycling energy and accumulating E_R than other sites. High EVI from the oak midstory (Roman et al., 2015) and lower wiregrass abundance at the intermediate site likely resulted in a greater decline in energy reserves compared to the xeric site when temperatures were above 35°C. Wiregrass, a C_4 species, can maintain photosynthetic capacity at high temperatures (Osborne and Sack, 2012; Ward et al., 1999), which is consistent with energy acquisition at the mesic and xeric sites. Furthermore, lower soil temperatures at the mesic site decreased heat stress and allowed for greater photosynthetic activity, and thus, the buildup of energy reserves.

A depletion in stored energy (i.e., negative E_R) demonstrated higher metabolic maintenance at the intermediate site corresponding to lower plant functional diversity and landscape homogenization (i.e., woody dominated understory; Western, 2001), thereby supporting our second hypothesis. The dense cover of broadleaf woody species in the understory, which is atypical for the longleaf pine ecosystem (Addington et al., 2006), increased basal E_M, which depleted energy reserves when elevated temperatures were prolonged (Yvon-Durocher et al., 2010). *Quercus margaretta*, a common understory shrub at the intermediate site, was shown to have lower water use and photosynthetic nitrogen-use efficiency compared to *Q. laevis* and *Q. incana* (Donovan *et al.*, 2000), which are more common at the xeric site. As a result, photosynthetic capacity was lower at the intermediate site with no apparent change in E_M, thereby decreasing energy reserves below that of the xeric site. Lower ecosystem function was especially pronounced when extreme heat events were cumulative, indicating limited adaptive capacity to environmental fluctuations at the intermediate site.

4.3. Metabolic entropy changes during cold and heatwave events

Reduced energy efficiency, as demonstrated by greater entropy exports at the intermediate and xeric sites relative to the mesic site, provides evidence of a decreased capacity to efficiently absorb and utilize solar energy (Brunsell et al., 2011). Higher entropy exports were especially pronounced during freeze events, suggesting that the leafless deciduous oak overstory was disadvantageous for the efficient utilization of incoming energy (Lenz et al., 2016). The intermediate site approached a steady state of entropy imports and exports when freeze was prolonged. This response was likely due to lower sensible heat fluxes (Wiesner et al., 2019), as T_{soil} was greater at the intermediate site during freezes (by ~2 °C), whereas T_{air} was lower compared to the other two sites, resulting in a lower temperature gradient at the site.

Overall, we observed greater energy efficiency during warmer months, suggesting that the ability to dissipate thermodynamic gradients greatly increased with higher leaf area (Wiesner et al., 2019). dS/dt did not indicate differences in energy efficiency during heatwaves among sites, suggesting greater influence of the physical gradients (i.e., VPD), and hydrology (i.e., rainfall, soil water availability) on entropy dissipation (Miralles et al., 2019). This result is in support of past findings in this ecosystem, where mesic and xeric sites showed similar hydraulic conductivity, due to higher root to leaf area ratios at more xeric sites (Addington et al., 2006; Ford, 2004).

4.4. Metabolic changes to hydrological drivers during temperature extremes

In partial support of our third hypothesis, we found that rainfall and soil moisture variation affected metabolic activity more at the intermediate and xeric sites, especially during freeze events. This result was somewhat surprising, as high clay contents at the mesic site led us to assume that changes in VWC during temperature extremes would decrease ecosystem function (Xu and Zhou, 2011). Lower E_A at the mesic site during heat events, but a more drastic increase in E_A in response to higher VWC during heatwave recovery, demonstrated greater metabolic plasticity of the plant species to changes in VWC (Drake et al., 2018; Hawkes et al., 2017). Greater plant functional diversity, specifically in the understory, likely increased function such that productivity could be maintained (Elmqvist et al., 2003). Accordingly, the mesic site could accumulate E_R in the event of lower available energy (Allen and Holling, 2010), which was especially evident when extreme events became cumulative, suggesting greater functional stability (Thompson et al., 2011). In contrast, plants at the xeric site were not adapted to high soil moisture following freeze events and prior to cold or heatwave events, as indicated by negative E_R (Ben-Noah and Friedman, 2018; Morales-Olmedo et al., 2015; van Bodegom et al., 2008).

Variation in metabolic functions to changes in VWC at the mesic and intermediate sites suggested that recovery was also a function of differences in soil characteristics (Mousavi et al., 2009; Saha and Kukal, 2015). The mesic site demonstrated a maintenance of metabolic function to alterations in VWC during freeze and greater energy reserve during the recovery from heat events as VWC increased. This response was a result of greater E_M, but lower E_A, at the intermediate site during heatwave recovery relative to the mesic and xeric sites. Both the mesic and xeric sites could maintain E_A at ~1 W m^{-2} during heat events when rainfall was high > 100 mm day^{-1}), in contrast to the intermediate site. Lower E_A at the intermediate site may be a function of tillage legacy, which altered the characteristics of the soil (Barlow et al., 2016; Hautier et al., 2015; Morris, 2010). Changes in the physical properties of the soil may have affected water percolation such that oxygen was depleted in the root zone when precipitation was high (Mousavi et al., 2009; Saha and Kukal, 2015). Higher E_A at the mesic and xeric sites also indicated higher transpiration rates maintained by metabolic function (Schymanski et al., 2013; Zandalinas et al., 2018).

The increase in E_M at xeric sites for heat events in response to greater

VWC demonstrated a rapid "disposal" of high soil water contents through evapotranspiration (Vivoni et al., 2008), which was at the cost of E_R. Greater drought tolerance at the xeric site, as shown by higher E_A compared to the other sites when VWC was below 18%, was promoted by plant species that have been shown to utilize greater proportions of groundwater (Addington et al., 2006; Ford, 2004) to maintain metabolic function during higher temperatures. In addition to utilizing groundwater, plant species at our xeric longleaf pine site exhibited more sensitive stomatal response compared to plants at the mesic longleaf sites (Addington et al., 2006; Ford, 2004). This response allowed for higher transpiration rates at the xeric site and also enabled higher tolerance to fluctuations in VWC during heatwaves (Seneviratne et al., 2010).

Savanna ecosystems are already facing considerable alterations across the globe and have been prone to environmental degradation that threatens their existence (Baudena et al., 2015; Devine et al., 2017; Mitchard and Flintrop, 2013; Mitchell et al., 2014). Weather anomalies may further alter the structure of these ecosystems through the expansion of woody species (Devine et al., 2017; Holmgren et al., 2013; Mitchard and Flintrop, 2013). Hardwood removal in mesic longleaf pine forests with greater oak abundance, specifically across Georgia, Alabama, Mississippi and the Carolinas, may improve resilience of these forests to future temperature extremes by lowering the metabolic demands of the ecosystem (Wiesner et al., 2020). In contrast oak species in more xeric longleaf pine forests may help maintain ecosystem function during heatwaves and droughts through greater transpiration rates (Schymanski et al., 2013; Zandalinas et al., 2018) if water is accessible (Wiesner et al., 2020), which can help reduce temperature gradients within the canopy (Westreenen et al., 2020) and promote energy reserves in parenchyma tissues (Sperling et al., 2017). This management strategy may help increase environmental resilience to temperature extremes in longleaf pine savannas across the Coastal Flatlands and xeric sandhills (i.e., Mississippi, Florida, Alabama) or on upland sites of the coastal plain.

5. Conclusions

We found that energy reserves in longleaf pine savannas are built during temperatures below 20 °C, and that high precipitation events impaired the ability of the ecosystem to build energy reserves following temperature extremes as a result of lower available energy and increased metabolic energy expenses. This response could have compounding effects on the ecosystem's ability to maintain its function if the co-occurrence of temperature and precipitation extremes become more frequent and could lead to greater alterations in community structure if the ability to store energy is compromised. Likewise, lower soil water availability decreased the ability to accumulate energy reserves at longleaf pine sites with greater oak overstory tree abundance.

Reductions in energy conservation and prolonged recovery, especially pronounced at sites with greater land use legacy (i.e., the intermediate site), suggest that severe modification of the natural environment can potentially reduce the "memory" effect from historic environmental fluctuations. As a result, plants did not reduce metabolic activity in response to lower resource availability during disturbances. Weather extremes may also increase the expansion of woody species. The maintenance of high metabolic activity of woody shrub and tree species during weather extremes could be unsustainable if resource availability continues to decrease with future changes in climate. Hardwood removal at longleaf pine forests with greater oak abundance and higher water availability may help to maintain resilience of these forests to temperature extremes by lowering the relative metabolic demands of the ecosystem.

Declaration of Competing Interest

The authors declare that they have no known competing financial interests or personal relationships that could have appeared to influence the work reported in this paper.

Acknowledgements

The authors thank the Forest Ecology laboratories personnel, with special thanks to Tanner Warren, Andres Baron-Lopez and Scott Taylor, for data collection and provision during the study at JWJERC. SW and GS acknowledge financial support from JWJERC. CS and GS acknowledge support from the U.S. National Science Foundation (DEB EF-1241881). CS and PS acknowledge support from the U.S. National Science Foundation (DEB EF-1702029). PS acknowledges support from the U.S. National Science Foundation (DEB 1552976).

Appendix

1. Entropy calculations

In the following we describe more detailed calculations for ecosystem entropy fluxes and production, referenced in section 2.7. The entropy flux of shortwave radiation (J_{Rs}, kJ m^{-2} K^{-1} day^{-1}) is:

$$J_{Rs} = R_{s,net} / T_{sun} \tag{A1}$$

where J_{Rs} is produced through the emission of shortwave radiation at the surface of the sun, with a surface temperature (T_{sun}) of ~5780 K. For the longwave radiation (J_{Rl}) flux in kJ m^{-2} K^{-1} day^{-1}, we calculated:

$$J_{Rl} = \left(R_{l,in} / T_{sky} - R_{l,out} / T_{srf}\right) \tag{A2}$$

The daily surface temperature (T_{srf} in K) was calculated from the upwelling longwave radiation as:

$$T_{srf} = R_{l,out} \Big/ \left(A \times e_{srf} \times k_B\right)^{\frac{1}{4}} \tag{A3}$$

Table A1
Average daily rainfall sums in mm, with standard deviations in parentheses, during cold wave event periods at the mesic, intermediate, and xeric sites.

Site	Pre	During	Post1	Post2	Post3	Post4	Post5
Mesic	2.37 (9.01)	0.66 (2.98)	4.30 (9.68)	4.74 (13.10)	4.92 (16.54)	4.13 (12.33)	2.49 (7.16)
Intermediate	1.78 (6.37)	0.60 (2.46)	3.36 (7.73)	4.90 (13.32)	2.51 (9.17)	3.16 (9.23)	2.33 (6.71)
Xeric	2.34 (10.11)	0.61 (2.84)	4.49 (10.06)	4.88 (12.00)	3.92 (14.28)	4.06 (11.98)	2.69 (8.75)

Table A2
Average daily rainfall sums in mm, with standard deviations in parentheses, during extreme heat event periods at the mesic, intermediate, and xeric sites.

Site	Pre	During	Post1	Post2	Post3	Post4	Post5
Mesic	2.72 (7.12)	2.44 (6.55)	3.25 (8.11)	2.83 (6.84)	3.23 (7.97)	2.67 (9.08)	2.96 (9.75)
Intermediate	2.37 (6.52)	1.80 (4.54)	2.76 (7.16)	2.27 (6.64)	1.80 (4.86)	1.95 (6.44)	2.14 (6.98)
Xeric	2.38 (6.67)	1.79 (4.37)	3.25 (8.17)	2.97 (6.9)	2.96 (7.35)	1.96 (6.15)	2.95 (10.56)

Table A3
Type 3 Tests of fixed effects for mixed models of freeze periods on metabolic response variables of average daily available Energy (E_A), metabolic energy (E_M), energy reserves E_R and mean daily entropy change (dS/dt).

Response	Effect	Chisq	Df	Pr(>Chisq)
E_A	(Intercept)	2.061	1	0.151
	Site	3.595	2	0.166
	Freeze ESP	7.797	6	0.253
	VWC	0.001	1	0.971
	VPD	102.313	1	<.0001
	Rain	25.307	1	<.0001
	T_{min}	14.878	1	<.0001
	Site:freeze ESP	27.657	12	0.006
	Freeze ESP:VPD	44.086	6	<.0001
	Freeze ESP:VWC	8.708	6	0.191
	Freeze ESP:Rain	79.116	6	<.0001
	Freeze ESP:T_{min}	22.944	6	0.001
	Site:Rain	57.644	2	<.0001
	Site:VWC	3.104	2	0.212
	Site:freeze ESP:VWC	24.646	12	0.017
E_M	(Intercept)	18.569	1	<.0001
	Site	16.35	2	<.0001
	Freeze ESP	59.918	6	<.0001
	VWC	1.404	1	0.236
	VPD	0.013	1	0.91
	Rain	23.877	1	<.0001
	INT	0.446	1	0.504
	T_{min}	113.27	1	<.0001
	Site:INT	6.585	2	0.037
	Site:freeze ESP	78.925	12	<.0001
	Freeze ESP:VPD	50.949	6	<.0001
	Freeze ESP:Rain	16.002	6	0.014
	Freeze ESP:T_{min}	169.414	6	<.0001
	Site:Rain	41.1	2	<.0001
	Site:VWC	21.92	2	<.0001
E_R	(Intercept)	1.032	1	0.31
	Site	6.228	2	0.044
	Freeze ESP	8.468	6	0.206
	VWC	0.068	1	0.794
	VPD	106.974	1	<.0001
	Rain	25.001	1	<.0001
	T_{min}	11.721	1	0.001
	Site:freeze ESP	27.773	12	0.006
	Freeze ESP:VPD	44.337	6	<.0001
	Freeze ESP:VWC	8.712	6	0.19
	Freeze ESP:Rain	79.826	6	<.0001
	Freeze ESP:T_{min}	22.028	6	0.001
	Site:Rain	45.935	2	0
	Site:VWC	5.775	2	0.056
	Site:freeze ESP:VWC	25.305	12	0.013
dS/dt	(Intercept)	0.254	1	0.615
	Site	2.188	2	0.335
	Freeze ESP	43.663	6	<.0001
	VPD	63.231	1	<.0001
	Rain	26.807	1	<.0001
	INT	0.29	1	0.59
	Cumulative effect	1.773	1	0.183
	VWC	1.434	1	0.231
	T_{min}	29.937	1	<.0001
	Site:Cumulative effect	8.627	2	0.013
	Site:INT	7.553	2	0.023
	Site:freeze ESP	40.158	12	<.0001
	Freeze ESP:VPD	64.08	6	<.0001
	Freeze ESP:T_{min}	41.227	6	<.0001
	Site:T_{min}	2.422	2	0.298
	Site:VPD	6.894	2	0.032
	Site:freeze ESP:T_{min}	29.655	12	0.003

Table A4
Type 3 Tests of fixed effects for mixed models of heatwave periods on metabolic response variables of average daily available Energy (E_A), metabolic energy (E_M), energy reserves E_R and mean daily entropy change (dS/dt).

Response	Effect	Chisq	Df	Pr(>Chisq)
E_A	(Intercept)	0.421	1	0.517
	Site	3.692	2	0.158
	Heatwave ESP	28.954	6	<.0001
	VWC	6.271	1	0.012
	VPD	37.303	1	<.0001
	Rain	7.546	1	0.006
	T_{max}	11.974	1	0.001
	INT	12.863	1	<.0001
	Site:INT	30.258	2	<.0001
	Site:heatwave ESP	20.243	12	0.063
	Heatwave ESP:VPD	21.536	6	0.001
	Heatwave ESP:VWC	21.433	6	0.002
	Heatwave ESP:Rain	44.794	6	<.0001
	Heatwave ESP:T_{max}	43.812	6	<.0001
	Site:VWC	4.473	2	0.107
	Site:heatwave ESP:VWC	23.166	12	0.026
E_M	(Intercept)	3.365	1	0.067
	Site	1.974	2	0.373
	Heatwave ESP	50.563	6	<.0001
	VWC	5.572	1	0.018
	VPD	8.623	1	0.003
	Rain	0.001	1	0.971
	INT	0.034	1	0.853
	Cumulative effect	4.27	1	0.039
	T_{max}	56.032	1	<.0001
	Site:INT	13.084	2	0.001
	Site:heatwave ESP	31.728	12	0.002
	Heatwave ESP:VPD	155.91	6	<.0001
	Heatwave ESP:Rain	38.323	6	<.0001
	Heatwave ESP:T_{max}	48.369	6	<.0001
	Site:T_{max}	17.733	2	<.0001
	Site:VWC	6.841	2	0.033
E_R	(Intercept)	5.582	1	0.018
	Site	5.456	2	0.065
	Heatwave ESP	34.43	6	<.0001
	VWC	32.535	1	<.0001
	VPD	35.522	1	<.0001
	Rain	9.578	1	0.002
	INT	12.828	1	<.0001
	T_{max}	9.381	1	0.002
	Site:INT	37.834	2	<.0001
	Site:heatwave ESP	29.14	12	0.004
	Heatwave ESP:VPD	20.694	6	0.002
	Heatwave ESP:VWC	43.434	6	<.0001
	Heatwave ESP:Rain	44.307	6	<.0001
	Heatwave ESP:T_{max}	14.282	6	0.027
	Site:T_{max}	1.99	2	0.37
	Site:VWC	7.896	2	0.019
	Site:heatwave ESP:T_{max}	24.051	12	0.02
dS/dt	(Intercept)	0.477	1	0.49
	Site	0.437	2	0.804
	Heatwave ESP	8.047	6	0.235
	VWC	16.625	1	<.0001
	VPD	37.882	1	<.0001
	Rain	0.303	1	0.582
	T_{max}	0.121	1	0.728
	Heatwave ESP:VPD	41.528	6	<.0001
	Heatwave ESP:Rain	18.417	6	0.005
	Heatwave ESP:T_{max}	14.337	6	0.026
	Site:Rain	14.614	2	0.001
	Site:VPD	14.183	2	0.001

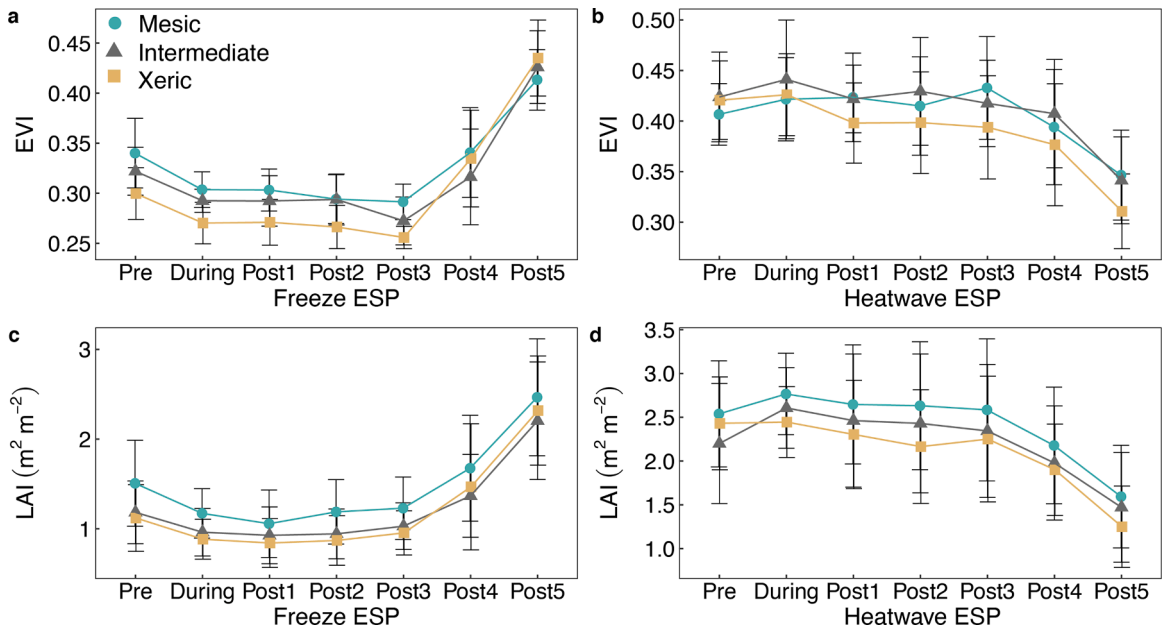

Figure A1. Average enhanced vegetation indices (a and b) and leaf area dynamics (c and d) with standard deviations, extracted from MODIS Aqua and Terra satellites reflectance data for cold (a and c) and heatwave (b and d) periods at the mesic, intermediate and xeric sites.

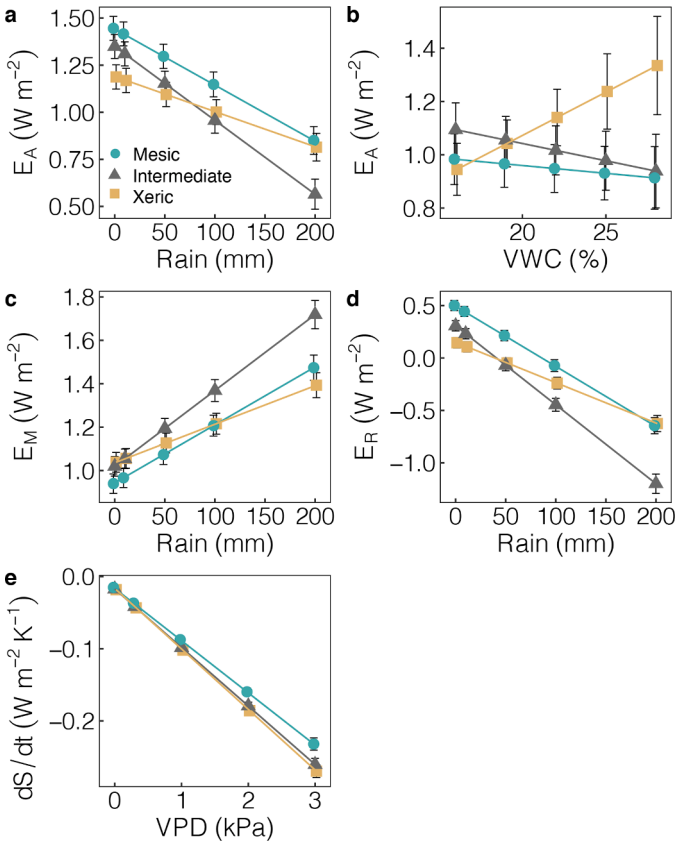

Figure A2. Least square mean predicted values from mixed model results as a function of environmental variables for freeze events by site. Site interactions with air temperature (T_{air} in °C), soil water content (VWC in %) and rainfall (in mm) on (a-c) energy reserves ($E_{reserves}$ in kJ m^{-2} day^{-1}), (d, e) the metabolic energy components (E_M/E_A), and (f, g) entropy production (dS/dt in kJ m^{-2} K^{-1} day^{-1}).

with the emissivity of the surface e_{srf} = 0.99-0.16α where α is the shortwave albedo (Juang et al., 2007), a surface area (A) of 1 m^2, and the Stefan-Boltzmann constant $k_B = 5.67 \times 10^{-8}$ W m^{-2} K^{-4}. The shortwave albedo (α) was calculated as the average daily ratio of noontime outgoing ($R_{s,out}$) and incoming ($R_{s,in}$) shortwave radiation. The daily sky temperature, T_{sky} (K), was likewise calculated from the incoming longwave radiation ($R_{L,in}$)

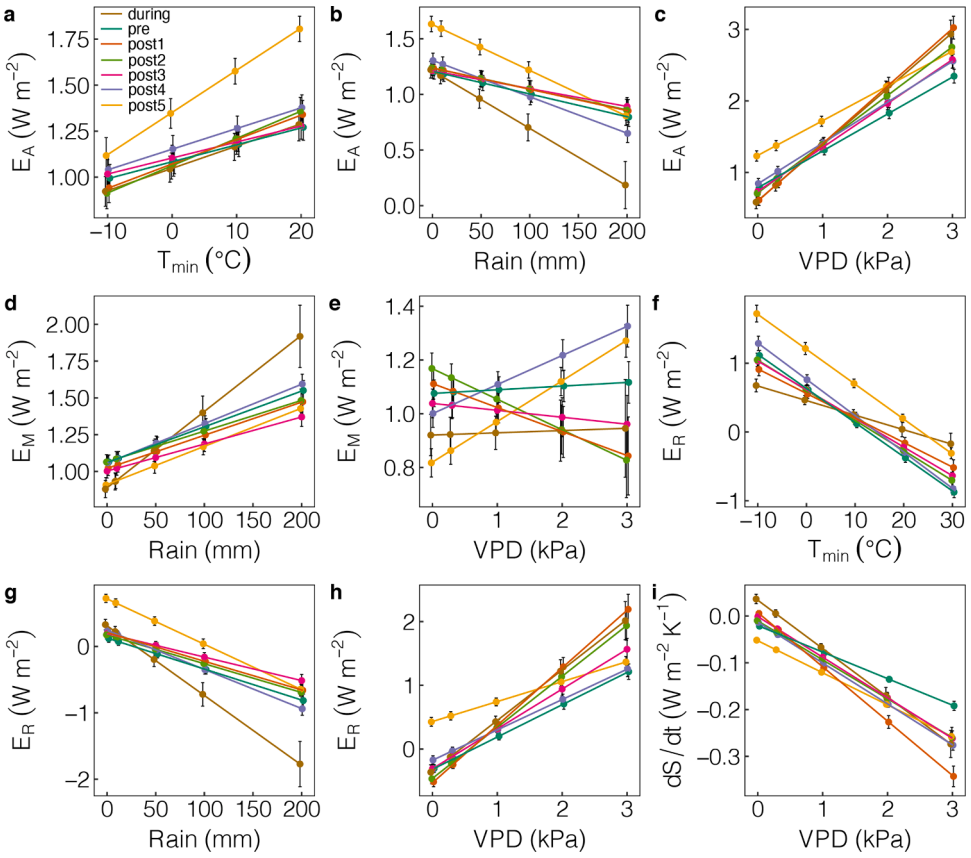

Figure A3. Least square mean predicted values from mixed model results of freeze event period (ESP) as a function of environmental variables by site. Site interactions on (a-c) energy reserves ($E_{reserves}$ in kJ m^{-2} day^{-1}) with (a) air temperature (T_{air} in °C), (b) soil water content (VWC in %) and (c) rainfall (in mm), (d-f) on the metabolic ratio (E_M/E_A) with (d) T_{air}, (e) VWC and (f) rainfall, as well as (g-i) entropy production (dS/dt in kJ m^{-2} K^{-1} day^{-1}) with (g) T_{air}, (h) VWC and (i) rainfall.

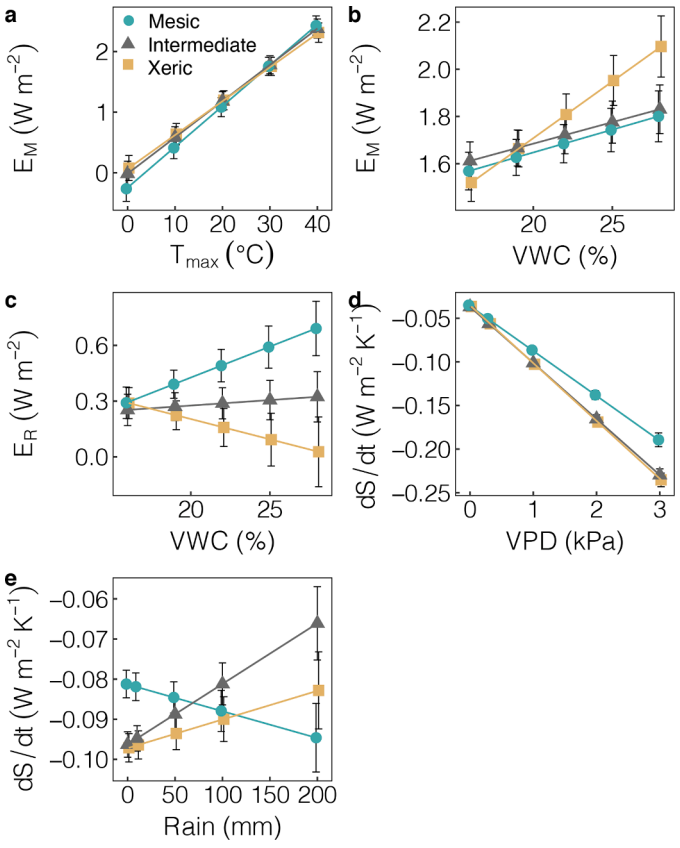

Figure A4. Least square mean predicted values from mixed model results as a function of environmental variables for heat events by site. Site interactions with air temperature (T_{air} in °C), soil water content (VWC in %) and rainfall (in mm) on (a-c) energy reserves ($E_{reserves}$ in kJ m^{-2} day^{-1}), (d-f) the metabolic energy components (E_M/E_A), and (g) entropy production (dS/dt in kJ m^{-2} K^{-1} day^{-1}).

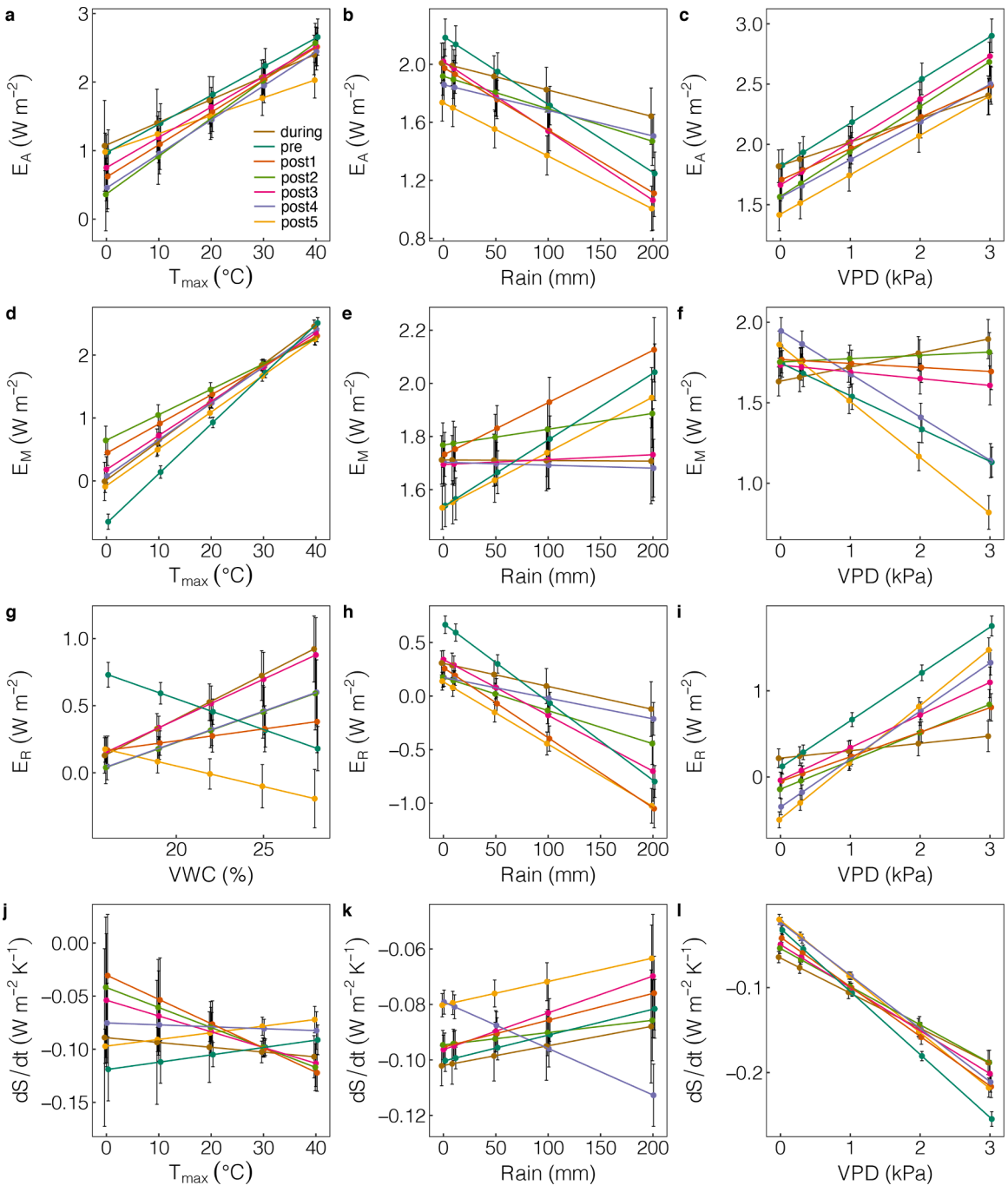

Figure A5. Least square mean predicted values from mixed model results of heat event period (ESP) as a function of environmental variables by site. Site interactions on (a-c) energy reserves ($E_{reserves}$ in kJ m^{-2} day^{-1}) with (a) air temperature (T_{air} in °C), (b) soil water content (VWC in %) and (c) rainfall (in mm), (d-f) on the metabolic ratio (E_M/E_A) with (d) T_{air}, (e) VWC and (f) rainfall, as well as (g-i) entropy production (dS/dt in kJ m^{-2} K^{-1} day^{-1}) with (g) T_{air}, (h) VWC and (i) rainfall.

using the Stefan-Boltzmann equation:

$$T_{sky} = R_{l,in} \Big/ (A \times e_{atm} \times k_B)^{\frac{1}{4}} \tag{A4}$$

where the emissivity of the atmosphere (e_{atm}) was assumed to be 0.85 following Campbell and Norman (1998), and A was likewise 1 m^2.

All ecosystem entropy fluxes, J_{LE}, J_H, J_G, J_{GEE}, and J_{Reco} in J m^{-2} K^{-1} day^{-1}, were calculated as:

$$J_x = x/T_y \tag{A5}$$

where x refers to the respective energy flux of LE, H, G, and NEE_e; and T_y is air temperature, or soil temperature for the calculation of J_G. Energy fluxes were converted from W m^{-2} to kJ m^{-2} and summed to daily estimates. We converted daily sums of NEE of CO_2 measured by the EC towers to energy

(NEE_e) assuming that 1 μmol of CO_2 assimilated stores 0.506 J in the biochemical reaction to form glucose as noted above. Accordingly, half hourly NEE was multiplied by 0.506 J and then summed to obtain a daily metabolic energy flux (Nikolov et al., 1995).

We also calculated the entropy produced associated with the mixing of saturated air from the canopy with air in the atmosphere during evaporation, when RH was below 100% (here calculated as a fraction), following Holdaway *et al.* (2010):

$$J_{LEmix} = ET \times R_v \times ln(RH) \quad \text{(A6)}$$

where the evapotranspiration rate (ET) was calculated as LE/λ, with λ as the latent heat of vaporization of water, and R_v as the gas constant of water vapor (0.461 kJ kg^{-1} K^{-1} for moist air). where

$$\sigma_{PAR} = FPAR \times (1/T_{air} - 1/T_{sun}) \quad \text{(A7)}$$

$$FPAR = EVI \times PAR \quad \text{(A8)}$$

$$\sigma_{Rs,leaf} = (R_s - PAR) \times (1/T_{air} - 1/T_{sun}) \times EVI \quad \text{(A9)}$$

$$\sigma_{Rl,leaf} = \sigma_{Rl} \times EVI \quad \text{(A10)}$$

References

Abu-Hamdeh, N.H., 2003. Thermal properties of soils as affected by density and water content. Biosystems Engineering 86, 97–102. https://doi.org/10.1016/s1537-5110(03)00112-0.

Addington, R.N., Donovan, L.A., Mitchell, R.J., Vose, J.M., Pecot, S.D., Jack, S.B., Hacke, U.G., Sperry, J.S., Oren, R., 2006. Adjustments in hydraulic architecture of Pinus palustris maintain similar stomatal conductance in xeric and mesic habitats. Plant Cell Environ 29, 535–545. https://doi.org/10.1111/j.1365-3040.2005.01430.x.

Aitken, S.N., Yeaman, S., Holliday, J.A., Wang, T., Curtis-McLane, S., 2008. Adaptation, migration or extirpation: climate change outcomes for tree populations. Evolutionary Applications 1, 95–111. https://doi.org/10.1111/j.1752-4571.2007.00013.x.

Alexander, L.V., 2016. Global observed long-term changes in temperature and precipitation extremes: A review of progress and limitations in IPCC assessments and beyond. Weather and Climate Extremes 11, 4–16. https://doi.org/10.1016/j.wace.2015.10.007.

Allen, C., Holling, C.S., 2010. Novelty, adaptive capacity, and resilience. Ecology & Society 15, 1–15. https://doi.org/10.5751/ES-03720-150324.

Alnsour, M., Ludwig-Müller, J., 2015. Potential effects of climate change on plant primary and secondary metabolism and its influence on plant ecological interactions. Journal of Endocytobiosis and Cell Research 26, 90–99.

Barlow, J., Lennox, G.D., Ferreira, J., Berenguer, E., Lees, A.C., Mac Nally, R., Thomson, J.R., de Barros Ferraz, S.F., Louzada, J., Oliveira, V.H.F., Parry, L., de Castro Solar, R.R., Vieira, I.C.G., Aragão, L.E.O.C., Begotti, R.A., Braga, R.F., Cardoso, T.M., de Oliveira, R.C., Souza Jr, C.M., Moura Jr, N.G., Nunes, S.S., Siqueira, J.V., Pardini, R., Silveira, J.M., Vaz-de-Mello, F.Z., Veiga, R.C.S., Venturieri, A., Gardner, T.A., 2016. Anthropogenic disturbance in tropical forests can double biodiversity loss from deforestation. Nature 535, 144–147. https://doi.org/10.1038/nature18326.

Bazot, S., Barthes, L., Blanot, D., Fresneau, C., 2013. Distribution of non-structural nitrogen and carbohydrate compounds in mature oak trees in a temperate forest at four key phenological stages. Trees 27, 1023–1034. https://doi.org/10.1007/s00468-013-0853-5.

Ben-Noah, I., Friedman, S.P., 2018. Review and evaluation of root respiration and of natural and agricultural processes of soil aeration. Vadose Zone Journal 17. https://doi.org/10.2136/vzj2017.06.0119, 0.

Beringer, J., Hacker, J., Hutley, L.B., LEUNING, R., Arndt, S.K., Amiri, R., Bannehr, L., Cernusak, L.A., Grover, S., Hensley, C., Hocking, D., Isaac, P., Jamali, H., Kanniah, K., Livesley, S., Neininger, B., U, K.T.P., Sea, W., Straten, D., Tapper, N., Weinmann, R., Wood, S., Zegelin, S., 2011. SPECIAL—Savanna patterns of energy and carbon integrated across the landscape. Bulletin of the American Meteorological Society 92, 1467–1485. https://doi.org/10.1175/2011bams2948.1.

Binkley, D., Stape, J.L., Ryan, M.G., 2004. Thinking about efficiency of resource use in forests. For. Ecol. Manage. 193, 5–16. https://doi.org/10.1016/j.foreco.2004.01.019.

Borghi, M., de Souza, L.P., Yoshida, T., Fernie, A.R., 2019. Flowers and climate change: a metabolic perspective. New Phyt 224, 1425–1441. https://doi.org/10.1111/nph.16031.

Boucek, R.E., Gaiser, E.E., Liu, H., Rehage, J.S., 2016. A review of subtropical community resistance and resilience to extreme cold spells. Ecosphere 7, e01455. https://doi.org/10.1002/ecs2.1455.

Braakman, R., Follows, M.J., Chisholm, S.W., 2017. Metabolic evolution and the self-organization of ecosystems. Proc Natl Acad Sci USA 114, E3091–E3100. https://doi.org/10.1073/pnas.1619573114.

Brunsell, N.A., Schymanski, S.J., Kleidon, A., 2011. Quantifying the thermodynamic entropy budget of the land surface: Is this useful? Earth Sys. Dyn 2, 87–103.

Campbell, G.S., Norman, C.G., 1998. An introduction to environmental biophysics. Springer.

Carturan, B.S., Parrott, L., Pither, J., 2018. A modified trait-based framework for assessing the resilience of ecosystem services provided by coral reef communities. Ecosphere 9, e02214. https://doi.org/10.1002/ecs2.2214.

Chapman, E.J., Childers, D.L., Vallino, J.J., 2015. How the second law of thermodynamics has informed ecosystem ecology through Its history. BioScience 66, 27–39. https://doi.org/10.1093/biosci/biv166.

Ciais, P., Reichstein, M., Viovy, N., Granier, A., Ogée, J., Allard, V., Aubinet, M., Buchmann, N., Bernhofer, C., Carrara, A., Chevallier, F., de Noblet, N., Friend, A.D., Friedlingstein, P., Grünwald, T., Heinesch, B., Keronen, P., Knohl, A., Krinner, G., Loustau, D., Manca, G., Matteucci, G., Miglietta, F., Ourcival, J.M., Papale, D., Pilegaard, K., Rambal, S., Seufert, G., Soussana, J.F., Sanz, M.J., Schulze, E.D., Vesala, T., Valentini, R., 2005. Europe-wide reduction in primary productivity caused by the heat and drought in 2003. Nature 437, 529–533. https://doi.org/10.1038/nature03972.

DAAC, ORNL., 2018. MODIS collection 5 land products global subsetting and visualization tool: NASA EOSDIS Land Processes DAAC. USGS Earth Resources Observation and Science EROS Center. https://doi.org/10.3334/ORNLDAAC/1379.

Domalski, E.S., Jobe, T.L.J., Milne, T.A., 1986. Thermodynamic data for biomass conversion and waste incineration (No. SERI/SP-271-2839.). National Bureau of Standards, Washington DC, Golden, CO. https://doi.org/10.2172/7038865.

Drake, J.E., Tjoelker, M.G., Vårhammar, A., Medlyn, B.E., Reich, P.B., Leigh, A., Pfautsch, S., Blackman, C.J., López, R., Aspinwall, M.J., Crous, K.Y., Duursma, R.A., Kumarathunge, D., De Kauwe, M.G., Jiang, M., Nicotra, A.B., Tissue, D.T., Choat, B., Atkin, O.K., Barton, C.V.M., 2018. Trees tolerate an extreme heatwave via sustained transpirational cooling and increased leaf thermal tolerance. Glob. Chang. Biol. 6, 129. https://doi.org/10.1111/gcb.14037.

Elmqvist, T., Folke, C., Nyström, M., Peterson, G., Bengtsson, J., Walker, B., Norberg, J., 2003. Response diversity, ecosystem change, and resilience. Front. Ecol. Environ. 1, 488–494. https://doi.org/10.1890/1540-9295(2003)001[0488:RDECAR]2.0.CO;2.

Ford, C.R., 2004. Variable distributions of water as a transpiration source: Consequences from the tree stem to ecosystem functioning. Diss. University of Georgia, Athens.

Francis, J.A., Vavrus, S.J., Cohen, J., 2017. Amplified Arctic warming and mid-latitude weather: new perspectives on emerging connections. Wiley Interdisciplinary Reviews: Climate Change 8, e474. https://doi.org/10.1002/wcc.474.

Frank, D., Reichstein, M., Bahn, M., Thonicke, K., Frank, D., Mahecha, M.D., Smith, P., Van Der Velde, M., Vicca, S., Babst, F., Beer, C., Buchmann, N., Canadell, J.G., Ciais, P., Cramer, W., Ibrom, A., Miglietta, F., Poulter, B., Rammig, A., Seneviratne, S.I., Walz, A., Wattenbach, M., Zavala, M.A., Zscheischler, J., 2015. Effects of climate extremes on the terrestrial carbon cycle: concepts, processes and potential future impacts. Glob. Chang. Biol. 21, 2861–2880. https://doi.org/10.1111/gcb.12916.

Goebel, P.C., Palik, B.J., Kirkman, L.K., Drew, M.B., West, L., Pederson, D.C., 2001. Forest ecosystems of a Lower Gulf Coastal Plain landscape: Multifactor classification and analysis. J. Torrey Bot. Soc. 128, 47. https://doi.org/10.2307/3088659.

Goebel, P.C., Palik, B.J., Kirkman, L.K., West, L., 1997. Field guide: Landscape ecosystem types of Ichauway. Joseph W. Jones Ecological Research Center at Ichauway, Newton. Report number 97–1.

Granier, A., Bréda, N., Biron, P., Villette, S., 1999. A lumped water balance model to evaluate duration and intensity of drought constraints in forest stands. Ecol. Model. 116, 269–283. https://doi.org/10.1016/s0304-3800(98)00205-1.

Groisman, P.Y., Bulygina, O.N., Yin, X., Vose, R.S., Gulev, S.K., Hanssen-Bauer, I., Førland, E., 2016. Recent changes in the frequency of freezing precipitation in North America and Northern Eurasia. Environ. Res. Lett. 11, 045007–045017. https://doi.org/10.1088/1748-9326/11/4/045007.

Hammond, G., Winnett, A., 2009. The influence of thermodynamic ideas on ecological economics: An interdisciplinary critique. Sustainability 1, 1195–1225. https://doi.org/10.3390/su1041195.

Hautier, Y., Tilman, D., Isbell, F., Seabloom, E.W., Borer, E.T., Reich, P.B., 2015. Anthropogenic environmental changes affect ecosystem stability via biodiversity. Monthley Weather Review 348, 336–340. https://doi.org/10.1126/science.aaa1788.

Hawkes, C.V., Waring, B.G., Rocca, J.D., Kivlin, S.N., 2017. Historical climate controls soil respiration responses to current soil moisture. Proc Natl Acad Sci USA 114, 6322–6327. https://doi.org/10.1073/pnas.1620811114.

Holdaway, R.J., Sparrow, A.D., Coomes, D.A., 2010. Trends in entropy production during ecosystem development in the Amazon Basin 1437–1447. doi:10.1098/rstb.2009.0298.

Huxman, T.E., Smith, M.D., Fay, P.A., Knapp, A.K., Shaw, M.R., Loik, M.E., Smith, S.D., Tissue, D.T., Zak, J.C., Weltzin, J.F., Pockman, W.T., Sala, O.E., Haddad, B.M., Harte, J., Koch, G.W., Schwinning, S., Small, E.E., Williams, D.G., 2004. Convergence across biomes to a common rain-use efficiency. Nature 429, 651–654. https://doi.org/10.1038/nature02561.

Juang, J.-Y., Katul, G., Siqueira, M., Stoy, P., Novick, K., 2007. Separating the effects of albedo from eco-physiological changes on surface temperature along a successional chronosequence in the southeastern United States. Geophysical Research Letters 34, 2415. https://doi.org/10.1029/2007GL031296.

Kaimal, J.C., Gaynor, J.E., 1991. Another look at sonic thermometry. Boundary-Layer Meteorol 56, 401–410. https://doi.org/10.1007/BF00119215.

Kirkman, L.K., Giencke, L.M., Taylor, R.S., Boring, L.R., Staudhammer, C.L., Mitchel, R. J., 2016. Productivity and species richness in longleaf pine woodlands: Resource-disturbance influences across an edaphic gradient. Ecology 97, 2259–2271. https://doi.org/10.1002/ecy.1456.

Kirkman, L.K., Mitchell, R.J., Helton, R.C., Drew, M.B., 2001. Productivity and species richness across an environmental gradient in a fire-dependent ecosystem. Am. J. Bot. 88, 2119–2128.

Kleidon, A., 2012. How does the Earth system generate and maintain thermodynamic disequilibrium and what does it imply for the future of the planet? Philos. Trans. R. Soc. Lond.: Mathematical, Physical and Engineering Sciences 370, 1012–1040. https://doi.org/10.1098/rsta.2011.0316.

Kleidon, A., 2010. A basic introduction to the thermodynamics of the Earth system far from equilibrium and maximum entropy production. Philosophical Transactions of the Royal Society B: Biological Sciences 365, 1303–1315. https://doi.org/10.1098/rstb.2009.0310.

Latimer, C.E., Zuckerberg, B., 2017. Forest fragmentation alters winter microclimates and microrefugia in human-modified landscapes. Ecography 40, 158–170. https://doi.org/10.1111/ecog.02551.

Lehmann, C.E.R., Archibald, S.A., Hoffmann, W.A., Bond, W.J., 2011. Deciphering the distribution of the savanna biome. New Phyt 191, 197–209. https://doi.org/10.1111/j.1469-8137.2011.03689.x.

Lenth, R.V., 2016. Least-Squares Means: The R Package lsmeans. J. Stat. Soft 69. https://doi.org/10.18637/jss.v069.i01.

Lenz, A., Hoch, G., Vitasse, Y., 2016. Fast acclimation of freezing resistance suggests no influence of winter minimum temperature on the range limit of European beech. Tree Phys 36, 490–501. https://doi.org/10.1093/treephys/tpv147.

Lin, H., 2015. Thermodynamic entropy fluxes reflect ecosystem characteristics and succession. Ecol. Model. 298, 75–86. https://doi.org/10.1016/j.ecolmodel.2014.10.024.

Lloyd, J., Taylor, J.A., 1994. On the temperature dependence of soil respiration. Functional Ecology 8, 315. https://doi.org/10.2307/2389824.

Makarieva, A.M., Gorshkov, V.G., Li, B.L., Chown, S.L., Reich, P.B., Gavrilov, V.M., 2008. Mean mass-specific metabolic rates are strikingly similar across life"s major domains: Evidence for life"s metabolic optimum. Proc Natl Acad Sci USA 105, 16994–16999. https://doi.org/10.1073/pnas.0802148105.

Malcolm, J.R., Markham, A., Neilson, R.P., Garaci, M., 2002. Estimated migration rates under scenarios of global climate change. Journal of Biogeography 29, 835–849. https://doi.org/10.1046/j.1365-2699.2002.00702.x.

Marshall, C.H., Pielke, R.A., Steyaert, L.T., 2003. Wetlands: crop freezes and land-use change in Florida. Nature 426, 29–30. https://doi.org/10.1038/426029a.

Martin-Benito, D., Anchukaitis, K., Evans, M., del Río, M., Beeckman, H., Cañellas, I., 2017. Effects of drought on xylem anatomy and water-use efficiency of two co-occurring pine species. Forests 8. https://doi.org/10.3390/f8090332, 332–19.

Miralles, D.G., Gentine, P., Seneviratne, S.I., Teuling, A.J., 2019. Land-atmospheric feedbacks during droughts and heatwaves: state of the science and current challenges. Ann. N. Y. Acad. Sci. 1436, 19–35. https://doi.org/10.1111/nyas.13912.

Morales-Olmedo, M., Ortiz, M., Sellés, G., 2015. Effects of transient soil waterlogging and its importance for rootstock selection. Chilean journal of agricultural research 75, 45–56. https://doi.org/10.4067/S0718-58392015000300006.

Morris, R.J., 2010. Anthropogenic impacts on tropical forest biodiversity: a network structure and ecosystem functioning perspective. Philosophical Transactions of the Royal Society B: Biological Sciences 365, 3709–3718. https://doi.org/10.1098/rstb.2010.0273.

Mousavi, S.F., Yousefi-Moghadam, S., Mostafazadeh-Fard, B., Hemmat, A., Yazdani, M. R., 2009. Effect of puddling intensity on physical properties of a silty clay soil under laboratory and field conditions. Paddy Water Environ 7, 45–54. https://doi.org/10.1007/s10333-008-0148-4.

NCDC, 2011. Monthly Station Normals of Temperature, Precipitation, and Heating and Cooling Degree Days 1981–2010. National Climatic Data center, Asheville, NC.

Nikolov, N.T., Massman, W.J., Schoettle, A.W., 1995. Coupling biochemical and biophysical processes at the leaf level: an equilibrium photosynthesis model for leaves of C3 plants. Ecol. Model. 80, 205–235. https://doi.org/10.1016/0304-3800(94)00072-P.

Osborne, C.P., Sack, L., 2012. Evolution of C4 plants: A new hypothesis for an interaction of CO2 and water relations mediated by plant hydraulics. Philosophical Transactions of the Royal Society B: Biological Sciences 367, 583–600. https://doi.org/10.1098/rstb.2011.0261.

Paruelo, J.M., Lauenroth, W.K., Burke, I.C., Sala, O.E., 1999. Grassland precipitation-use efficiency varies across a resource gradient. Ecosystems 2, 64–68. https://doi.org/10.1007/s100219900058.

Peñuelas, J., Sardans, J., Filella, I., Estiarte, M., Llusià, J., Ogaya, R., Carnicer, J., Bartrons, M., Rivas-Ubach, A., Grau, O., Peguero, G., Margalef, O., Pla-Rabés, S., Stefanescu, C., Asensio, D., Preece, C., Liu, L., Verger, A., Rico, L., Barbeta, A., Achotegui-Castells, A., Gargallo-Garriga, A., Sperlich, D., Farré-Armengol, G., Fernández-Martínez, M., Liu, D., Zhang, C., Urbina, I., Camino, M., Vives, M., Nadal-Sala, D., Sabate, S., Gracia, C., Terradas, J., 2018. Assessment of the impacts of climate change on Mediterranean terrestrial ecosystems based on data from field experiments and long-term monitored field gradients in Catalonia. Environmental and Experimental Botany 152, 49–59. https://doi.org/10.1016/j.envexpbot.2017.05.012.

Pielke, R.A., Mahmood Sr, R., McAlpine, C., 2016. Land's complex role in climate change. Physics Today 69, 40–46. https://doi.org/10.1063/PT.3.3364.

Pugnaire, F.I., Morillo, J.A., Peñuelas, J., Reich, P.B., Bardgett, R.D., Gaxiola, A., Wardle, D.A., van der Putten, W.H., 2019. Climate change effects on plant-soil feedbacks and consequences for biodiversity and functioning of terrestrial ecosystems. Science Advances 5 eaaz1834.

R Core Team, 2013. R: A Language and Environment for Statistical Computing.

Rahmstorf, S., Coumou, D., 2011. Increase of extreme events in a warming world. Proc Natl Acad Sci USA 108, 17905–17909. https://doi.org/10.1073/pnas.1101766108.

Reichstein, M., Bahn, M., Mahecha, M.D., Kattge, J., Baldocchi, D.D., 2014. Linking plant and ecosystem functional biogeography. Proc Natl Acad Sci USA 111, 13697–13702. https://doi.org/10.1073/pnas.1216065111.

Reichstein, M., Tenhunen, J., Roupsard, O., Ourcival, J.-M., Rambal, S., Miglietta, F., Peressotti, A., Pecchiari, M., Tirone, G., Valentini, R., 2003. Inverse modeling of seasonal drought effects on canopy CO_2/H_2O exchange in three Mediterranean ecosystems. J. Geophys. Res. Atmos 108, 1879. https://doi.org/10.1029/2003JD003430.

Richardson, A.D., Black, T.A., Ciais, P., Delbart, N., Friedl, M.A., Gobron, N., Hollinger, D.Y., Kutsch, W.L., Longdoz, B., Luyssaert, S., Migliavacca, M., Montagnani, L., Munger, J.W., Moors, E., Piao, S., Rebmann, C., Reichstein, M., Saigusa, N., Tomelleri, E., Vargas, R., Varlagin, A., 2010. Influence of spring and autumn phenological transitions on forest ecosystem productivity. Philosophical Transactions of the Royal Society B: Biological Sciences 365, 3227–3246. https://doi.org/10.1098/rstb.2010.0102.

Richardson, A.D., Keenan, T.F., Migliavacca, M., Ryu, Y., Sonnentag, O., Toomey, M., 2013. Climate change, phenology, and phenological control of vegetation feedbacks to the climate system. Agric. For. Meteorol. 169, 156–173. https://doi.org/10.1016/j.agrformet.2012.09.012.

Rodrigues, T.R., Vourlitis, G.L., de, A, Lobo, F., de Oliveira, R.G., de, S, Nogueira, J., 2014. Seasonal variation in energy balance and canopy conductance for a tropical savanna ecosystem of South Central Mato Grosso. Journal of Geophysical Research: Biogeosciences 119, 1–13. https://doi.org/10.1002/2013jg002472.

Roman, D.T., Novick, K.A., Brzostek, E.R., Dragoni, D., Rahman, F., Phillips, R.P., 2015. The role of isohydric and anisohydric species in determining ecosystem-scale response to severe drought. Oecologia 179, 641–654. https://doi.org/10.1007/s00442-015-3380-9.

Saha, D., Kukal, S.S., 2015. Soil structural stability and water retention characteristics under Different Land uses of Degraded Lower Himalayas of North-West India. Land Degradation & Development 26, 263–271.

Savi, T., Bertuzzi, S., Branca, S., Tretiach, M., Nardini, A., 2014. Drought-induced xylem cavitation and hydraulic deterioration: risk factors for urban trees under climate change? New Phyt 205, 1106–1116. https://doi.org/10.1111/nph.13112.

Schneider, E.D., Kay, J.J., 1994. Life as a manifestation of the second law of thermodynamics. Math. Comput. Mod. 19, 25–48. https://doi.org/10.1016/0895-7177(94)90188-0.

Schobert, H.H., 2013. Chemistry of Fossil Fuels and Biofuels (Cambridge Series in Chemical Engineering). Cambridge: Cambridge University Press. https://doi.org/10.1017/CBO9780511844188.

Schymanski, S.J., Or, D., Zwieniecki, M., 2013. Stomatal control and leaf thermal and hydraulic capacitances under rapid environmental fluctuations. PLoS ONE 8, e54231. https://doi.org/10.1371/journal.pone.0054231.

Seneviratne, S.I., Corti, T., Davin, E.L., Hirschi, M., Jaeger, E.B., Lehner, I., Orlowsky, B., Teuling, A.J., 2010. Investigating soil moisture–climate interactions in a changing climate: A review. Earth-Science Reviews 99, 125–161. https://doi.org/10.1016/j.earscirev.2010.02.004.

Sevanto, S., Mcdowell, N.G., DICKMAN, L.T., PANGLE, R., Pockman, W.T., 2013. How do trees die? A test of the hydraulic failure and carbon starvation hypotheses. Plant Cell Environ 37, 153–161. https://doi.org/10.1111/pce.12141.

Silva, C.S., Seider, W.D., Lior, N., 2015. Exergy efficiency of plant photosynthesis. Chemical Engineering Science 130, 151–171.

Sippela, S., Zscheischlerb, J., Reichsteina, M., 2016. Ecosystem impacts of climate extremes crucially depend on the timing. Proc Natl Acad Sci USA 113, 5768–5770. https://doi.org/10.1073/pnas.1605667113.

Sperling, O., Silva, L.C.R., Tixier, A., Théroux-Rancourt, G., Zwieniecki, M.A., 2017. Temperature gradients assist carbohydrate allocation within trees. Sci. Rep. 7, 1–10. https://doi.org/10.1038/s41598-017-03608-w.

Starr, G., Staudhammer, C.L., Wiesner, S., Kunwor, S., Loescher, H.W., Baron, A.F., Whelan, A., Mitchell, R.J., Boring, L., 2016. Carbon dynamics of *Pinus palustris* ecosystems following drought. Forests 7, 98. https://doi.org/10.3390/f7050098.

Staver, A.C., 2017. Prediction and scale in savanna ecosystems. New Phyt 219, 52–57. https://doi.org/10.1111/nph.14829.

Stoy, P.C., Lin, H., Novick, K.A., Siqueira, M.B.S., Juang, J.-Y., 2014. The role of vegetation on the ecosystem radiative entropy budget and trends along ecological succession. Entropy 16, 3710–3731. https://doi.org/10.3390/e16073710.

Thompson, I.D., Okabe, K., Tylianakis, J.M., Kumar, P., Brockerhoff, E.G., Schellhorn, N. A., Parrotta, J.A., Nasi, R., 2011. Forest biodiversity and the delivery of ecosystem goods and services: Translating science into policy. BioScience 61, 972–981. https://doi.org/10.1525/bio.2011.61.12.7.

Twine, T.E., Kustas, W.P., Norman, J.M., Cook, D.R., Houser, P.R., Meyers, T.P., Prueger, J.H., Wesley, M.L., 2000. Correcting eddy covariance flux underestimates over grassland. Agric. For. Meteorol. 103, 279–300. https://doi.org/10.1016/S0168-1923(00)00123-4.

van Bodegom, P.M., Sorrell, B.K., Oosthoek, A., Bakker, C., Aerts, R., 2008. Separating the effects of partial submergence and soil oxygen demand on plant physiology. Ecology 89, 193–204. https://doi.org/10.1890/07-0390.1.

Villanueva, M.C., 2015. Contrasting tropical estuarine ecosystem functioning and stability: A comparative study. Estuarine. Coastal and Shelf Science 155, 89–103. https://doi.org/10.1016/j.ecss.2014.12.044.

Vivoni, E.R., Moreno, H.A., Mascaro, G., Rodriguez, J.C., Watts, C.J., Payan, J.G., Scott, R.L., 2008. Observed relation between evapotranspiration and soil moisture in the North American monsoon region. Geophysical Research Letters 35, 7251. https://doi.org/10.1029/2008GL036001.

Ward, J.K., Tissue, D.T., Thomas, R.B., Strain, B.R., 1999. Comparative responses of model C3 and C4 plants to drought in low and elevated CO2. Glob. Chang. Biol. 5, 857–867. https://doi.org/10.1046/j.1365-2486.1999.00270.x.

Western, D., 2001. Human-modified ecosystems and future evolution. Proc Natl Acad Sci USA 98, 5458–5465. https://doi.org/10.1073/pnas.101093598.

Westreenen, A.V., Zhang, N., Douma, J.C., Evers, J.B., Anten, N.P.R., Marcelis, L.F.M., 2020. Substantial differences occur between canopy and ambient climate: Quantification of interactions in a greenhouse-canopy system. PLoS ONE 15, e0233210. https://doi.org/10.1371/journal.pone.0233210.

Whelan, A., Mitchell, R., Staudhammer, C., Starr, G., 2013. Cyclic occurrence of fire and its role in carbon dynamics along an edaphic moisture gradient in longleaf pine ecosystems. PLoS ONE 8, e54045. https://doi.org/10.1371/journal.pone.0054045.

Wiesner, S., Staudhammer, C.L., Stoy, P.C., Boring, L.R., Starr, G., 2019. Quantifying energy use efficiency via entropy production: A case study from longleaf pine ecosystems. Biogeosciences 16, 1845–1863.

Wiesner, S., Stoy, P.C., Staudhammer, C.L., Starr, G., 2020. Using metabolic energy density metrics to understand differences in ecosystem function during drought. Journal of Geophysical Research: Biogeosciences 125, 1443. https://doi.org/10.1029/2019JG005335.

Wilson, C.A., Mitchell, R.J., Hendricks, J.J., Boring, L.R., 1999. Patterns and controls of ecosystem function in longleaf pine - wiregrass savannas. II. Nitrogen dynamics. Can. J. For. Res. 29, 752–760. https://doi.org/10.1139/x99-050.

Wolf, S., Keenan, T.F., Fisher, J.B., Baldocchi, D.D., Desai, A.R., Richardson, A.D., Scott, R.L., Law, B.E., Litvak, M.E., Brunsell, N.A., Peters, W., van der Laan-Luijkx, I. T., 2016. Warm spring reduced carbon cycle impact of the 2012 US summer drought. Proc Natl Acad Sci USA 113, 5880–5885. https://doi.org/10.1073/pnas.1519620113.

Xie, Y., Wang, X., Silander, J.A., 2015. Deciduous forest responses to temperature, precipitation, and drought imply complex climate change impacts. Proc Natl Acad Sci USA 112, 13585–13590. https://doi.org/10.1073/pnas.1509991112.

Xu, Z., Zhou, G., 2011. Responses of photosynthetic capacity to soil moisture gradient in perennial rhizome grass and perennial bunchgrass. BMC Plant Biology 11, 21. https://doi.org/10.1186/1471-2229-11-21.

Yvon-Durocher, G., Jones, J.I., Trimmer, M., Woodward, G., Montoya, J.M., 2010. Warming alters the metabolic balance of ecosystems. Philosophical Transactions of the Royal Society B: Biological Sciences 365, 2117–2126. https://doi.org/10.1098/rstb.2010.0038.

Zandalinas, S.I., Mittler, R., Balfagón, D., Arbona, V., Cadenas, A.G., 2018. Plant adaptations to the combination of drought and high temperatures. Physiologia plantarum 162, 2–12.

Zscheischler, J., Westra, S., van den Hurk, B.J.J.M., Seneviratne, S.I., Ward, P.J., Pitman, A., AghaKouchak, A., Bresch, D.N., Leonard, M., Wahl, T., Zhang, X., 2018. Future climate risk from compound events. Nature Climate Change 8, 469–477. https://doi.org/10.1038/s41558-018-0156-3.